

Inconsistent metallicity spreads in first generation stars of globular clusters from high resolution spectroscopy and HST photometry

Eugenio Carretta¹ and Angela Bragaglia¹

INAF-Osservatorio di Astrofisica e Scienza dello Spazio di Bologna, Via P. Gobetti 93/3, I-40129 Bologna, Italy

ABSTRACT

An open issue about multiple stellar populations in globular clusters (GCs) is the possible existence of metallicity spreads in first generation (FG) stars. Recent estimates based on HST pseudo-colours map (PCM) derived unlikely large spreads in [Fe/H] from spreads in the colour $col = m_{F275W} - m_{F814W}$. The inferred metallicity spreads for many GCs are comparable or even larger than those observed in dwarf galaxies. This result is clearly unexpected and at odds with the birth time of stars in dwarf galaxies, spanning several billion years, as opposed to very short formation times of the stellar component in GCs (a few million years). The contradiction is corroborated by the comparison of the widths of red giant branches in both classes of objects. Moreover, the so called spreads in FG stars estimated from the PCMs are always larger than the intrinsic metallicity spreads derived from spectroscopy. We used 30 pairs of FG stars with similar parameters in 12 GCs to highlight that a constant displacement in Δcol corresponds to variable differences in [Fe/H] up to 0.2 dex, depending on the GC. Providing for the first time quantitative measurements of the extension in Δcol of the sequences of FG and SG stars, we found no relation between metallicity spreads previously derived and extension of FG stars. We found that the length of the FG region correlates with the average global metallicity of GCs, and not with the observed metallicity spreads. The extension of FG stars also correlates with the extension of SG stars, and the global mass of the GCs. Our findings seriously challenge the scenario claiming more inhomogeneous mixing among FG stars, invalidating previous speculations in the literature.

Key words. Stars: abundances – Stars: atmospheres – Stars: Population II – Galaxy: globular clusters: general

1. Introduction

A still unsolved issue on multiple populations (MPs) in globular clusters (GCs) concerns the possible existence of metallicity spreads among first generation (FG) stars. These stars formed in the primary star formation phase at the very beginning of the lifetime of these old stellar systems, shortly after the Big Bang (e.g., Carretta et al. 2000, VandenBerg et al. 2013). As hinted by their narrow photometric sequences in the colour-magnitude diagrams (CMDs), GCs do not have an extended star formation. In particular, FG stars have an abundance pattern analogous to field halo stars of similar metallicity, bearing traces only of supernovae (SNe) nucleosynthesis, that is enhanced levels of α -elements typical of contributions from massive stars exploding as core-collapse SNe. Type Ia SNe, with their longer evolving times, do not provide a noticeable contribution to the chemistry of most GCs, as proven by the homogeneity of Fe-peak species in the majority of GCs (better than 12% or less than 0.05 dex, Carretta et al. 2009a; see also, e.g., Bailin and von Klarmann 2022, Willman and Strader 2012). The most massive objects among FG stars provide the nuclearly processed matter, enriched in proton-capture elements

from H-burning at high temperature, that together with varying amounts of pristine gas produce the chemical composition typical of second generation (SG) stars (e.g., Langer et al. 2003, Gratton et al. 2001), although the exact nature of the polluters is still debated (e.g., the reviews by Gratton et al. 2004, 2012, 2019, and Bastian and Lardo 2018).

First generation stars can be easily separated from SG stars directly, deriving their abundances with spectroscopy. The chief disadvantage is represented by the time consuming observations, albeit mitigated by the use of efficient spectrographs with high multiplexing gain at large telescopes. The tagging of MPs can also be indirectly performed by photometric means, exploiting the effect of different abundances involved in the H-burning on filters at the bandpasses appropriate to sample spectral regions where main molecular bands associated to CNO products are located. With the benefit of sampling many more stars in a short time, photometric methods have the main handicap to follow primarily the N abundance, obtained using filters encompassing the ultraviolet or blue regions where NH or CN features are located (e.g., Calamida et al. 2007, Sbordone et al. 2011, Carretta et al. 2011a, Lardo et al. 2011, Lee et al. 2009, Milone et al. 2017, Johnson et al. 2023). Hence, the photometric approach essentially measures the N content in differ-

Send offprint requests to: E. Carretta, eugenio.carretta@inaf.it

ent populations and is prone to some ambiguity, since N can be generated by the conversion of C for temperatures above 10 MK, but also from O when the ON branch of the CNO cycle is activated at higher temperatures.

Discrepancies between the spectroscopic and the photometric approaches in tagging MPs are examined in Carretta and Bragaglia (2024; hereinafter CB24), using pseudo-colour maps (PCMs) and high resolution spectroscopy for 22 GCs. We showed that PCMs are able to provide a coarse division of MPs, with FG and SG stars usually separated into two groups, with an efficient trade off between limited observing time and number of surveyed stars. However, we found that photometric methods tend to overestimate the fraction of FG stars, with the number of mismatches depending on the GC mass (CB24). This happens both with ground-based and space-based photometry.

The results by CB24 suggest that the photometric approach is sound, in broad terms, but maybe still not completely understood. Many of the conclusions based on PCMs seem still based on empirical evidence and some inferences may be misleading.

In the present paper we use the sample of PCMs by CB24, the only published so far, to explore in details the claims of the possible existence of a metallicity spread among FG stars. Our purposes are to ascertain whether a spread in $[\text{Fe}/\text{H}]$ is truly connected to the extension of the region of FG stars in the PCM, whether the spread in the region of SG stars also indicates a metallicity dispersion in this population, and finally to disclose potential inconsistencies between spectroscopy and HST photometry in this issue regarding MPs.

For clarity, in Table 1, adapted from CB24, we reproduce the simplified notation to describe the PCMs, whose detailed description can be found in Milone et al. (2017: M17). Here we added the definition of $RG1$ as the region in the PCM populated by FG stars, and analogously $RG2$ as the locus in the PCM with the preponderant presence of SG stars.

The problem of possible metallicity spreads among GC stars seems to be primarily based on indirect inferences. None of the candidate polluters proposed as sources of matter enriched in proton-capture elements produces also variations in metallicity, so the $[\text{Fe}/\text{H}]$ content of MPs is expected to be very homogeneous, as supported by the cosmic scatter of iron in GCs (e.g., Carretta et al. 2009a). However, from the PCMs of 55 GCs, still unpublished, M17 state that the extension of the $RG1$ (see Tab. 1) is too large if compared to the photometric errors obtained by bootstrap technique. Milone et al. (2017) claim that this comparison implies that FG stars may have a dishomogeneous composition. Since the x-coordinate (Δcol) in the PCMs is mainly sensitive to variations in effective temperature of stars (through the differential use of a long baseline colour), changes in He content or in metallicity were proposed as responsible for the observed spread. Since FG stars should not have an enhanced He level due to H-burning in massive polluters, Milone et al. argue that the extension of $RG1$ along Δcol is entirely due to metallicity variations.

Legnardi et al. (2022: L22) extend the work of M17, who only considered red giant branch (RGB) stars, to the main sequence (MS) of two GCs (NGC 6362, NGC 6838), also observed with HST in the same filters. They find essentially the

Table 1. Notation adopted in the present paper

$col = mag_{F275W} - mag_{F814W}$
$col3 = (mag_{F275W} - mag_{F336W}) - (mag_{F336W} - mag_{F438W})$
$\Delta col = W_{col}((col - xr)/(xr - xb))$
$\Delta col3 = W_{col3}((col3 - yr)/(yr - yb))$ (see Section 2)
W_{col} and W_{col3} = widths of the RGB in col and $col3$
PCM = pseudo-colour map = Δcol in abscissa and $\Delta col3$ in ordinate
$RG1$ = region in the PCM populated by FG stars only
$RG2$ = region in the PCM populated by SG (or non-FG) stars
$lenRG1$ = extension of the $RG1$ region in Δcol
$iqrSG$ = extension of the $RG2$ region in Δcol

same results for RGB and MS stars, that is a separation between $RG1$ and $RG2$ (although clearer on the RGB due to the much smaller photometric errors) and an elongation of the $RG1$ distribution in Δcol larger than that of $RG2$ and of estimated errors. They further check the possibility that such a spread could be due to the presence of binaries or a spread in helium. As for M17, the latter occurrence is difficult to reconcile with the fact that these stars represent the primordial population of the GC, without any chemical variations due to polluters. Based on simulations, they discard the two explanations and attribute the spread in Δcol solely to a spread in metallicity. They then proceed to translate the width of FG stars on the RGB measured by M17, i.e., $W1g = W_{F275W, F814W}^{1G}$ to a spread in metallicity, using the colour-metallicity relations of Dotter et al. (2008). This procedure results in spreads from about 0.05 to 0.3 dex (their Table 3).

In the present paper we first highlight the inconsistency of metallicity spreads in FG stars as derived in L22 from the PCMs with the observed dispersions in $[\text{Fe}/\text{H}]$ from high resolution spectroscopy (Section 2). We then use a large set of stars identified with spectroscopic criteria as FG stars in 20 GCs (CB24) to analyse the discrepancies between spectroscopy and HST photometry and to investigate the dependence of the coordinate Δcol on $[\text{Fe}/\text{H}]$, providing empirical constraints to the true rate of changes in both metallicity and Δcol (Section 3). In Section 4 we quantify for the first time the real extension of the sequence of FG stars in the PCM. These precise measurements are compared with global parameters of GCs to study dependences and possible correlations. Section 5 is devoted to scrutinising the existence of possibly neglected metallicity spreads among SG stars. Finally, in Section 6 we present our conclusions and further implications of our findings.

2. Metallicity spreads of GC FG stars in context

From the extension in Δcol of the $RG1$ in the unpublished PCMs of GCs, L22 advocate that metallicity spreads must be present among the stars born in the primary star formation within GCs. The magnitude of the spread derived for many GCs is significantly overestimated using their approach. The values of the the metallicity spread attributed by L22 to FG stars are generally too large for stellar systems long known to be homogeneous in heavy elements, as supported by their narrow photometric sequences in the CMDs.

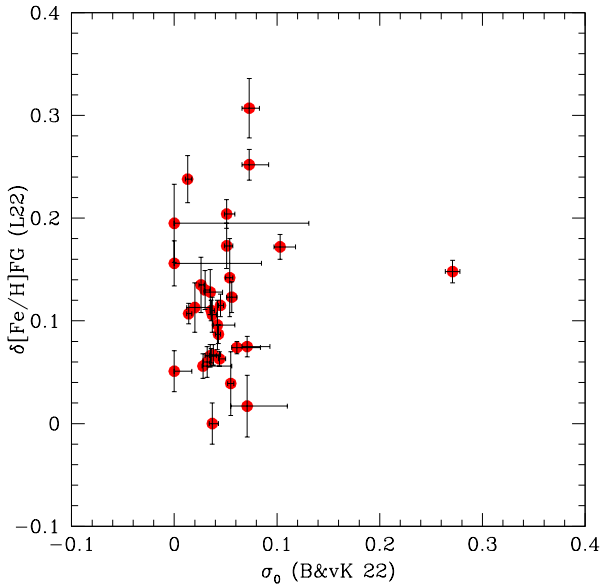


Fig. 1. Metallicity spreads for FG stars derived from PCMs by L22 as a function of the intrinsic dispersion in $[\text{Fe}/\text{H}]$ calculated in Bailin and von Klar (2022) for 33 GCs in common.

To better visualise this inconsistency, in Fig. 1 we compare the estimates by L22, $\delta[\text{Fe}/\text{H}]_{\text{FG}}$, to the intrinsic metallicity dispersions obtained by Bailin and von Klar (2022). They update the estimates of Bailin (2019) of the internal dispersion σ_0 from high resolution spectroscopy of RGB stars, taking into account both random and systematic errors associated to the abundance analysis. The values by Bailin and von Klar are referred to the total internal spread in iron abundance, without distinction between FG and SG stars.

With the notable exception of ω Cen, the intrinsic iron spreads in GCs are usually small, mostly below 0.1 dex. In contrast, FG spreads derived in L22 show a long tail extending to dispersions in $[\text{Fe}/\text{H}]$ as large as 0.2–0.3 dex, the record being NGC 5024, with a spread of 0.307 dex.

Only 33 GCs are in common between the studies of L22 and Bailin and von Klar (2022). Furthermore, for some GCs the number of stars with abundance analysis from high resolution spectroscopy is limited. A more complete and instructive view for the soundness of the estimates by L22 is provided in Fig. 2, where the spreads in $[\text{Fe}/\text{H}]$ for FG stars in all the 55 GCs analysed in L22 (open black squares) are plotted as a function of the total absolute magnitude of the GCs, a proxy for the present-day total stellar mass, from Harris (2010). In the same figure a variety of other stellar systems from the compilation by Willman and Strader (2012) are also reported. To explore a meaningful definition for “galaxy”, they used a Bayesian Markov Chain Monte Carlo technique to derive consistent intrinsic metallicity spreads for 24 GCs and 16 dwarf galaxies and satellites of the Milky Way. The GCs considered are mostly from our homogeneous FLAMES survey of large sample of stars in GCs (Carretta et al. 2009b), plus other literature data for M 22 and ω Cen. Complete references for the sample of dwarfs can be found in Willman and Strader (2012).

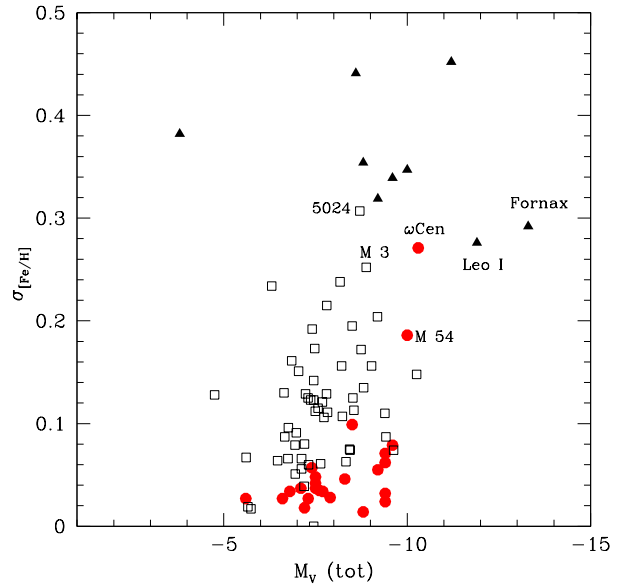


Fig. 2. Spread in $[\text{Fe}/\text{H}]$ for FG stars in 55 GCs (black open squares) as a function of the GC present-day mass as expressed by the total absolute magnitude M_V (Harris 2010). Metallicity spreads are derived from PCMs by L22. Filled red circles and black triangles are spectroscopic $\sigma_{[\text{Fe}/\text{H}]}$ of GCs and dwarf galaxies, respectively, from Willman and Strader (2012). A few interesting objects are labelled in the figure.

From Fig. 2, several conclusions can be drawn. First, also in this figure the vast majority of $[\text{Fe}/\text{H}]$ spreads advocated for a limited fraction of stars (the FG stars) in each GC are much larger than the estimates obtained from spectroscopic observations of the GCs as whole systems. Second, it is not clear whether a trend as a function of mass is present for the values by L22, whereas an increase of the global spread for GCs of increasingly larger mass is rather evident. Third, and most astonishing, a few estimates by L22 are comparable to or even exceed the metallicity dispersion observed in much more massive dwarf galaxies.

In particular, this is true for the values derived by L22 for NGC 5024 (M 53) and NGC 5272 (M 3), with $\delta[\text{Fe}/\text{H}]_{\text{FG}}=0.307$ and 0.252 dex, respectively. These are exceptionally large amounts, since both M 53 (Boberg et al. 2016) and M 3 (Cohen and Melendez 2005, Sneden et al. 2004) are GCs known to be extremely homogeneous in the abundance of heavy elements. According to L22, NGC 5024 would host among its FG stars a metallicity spread larger than the one detected in ω Cen¹. In addition, several GCs in Fig. 2, including M 53 and M 3, have a spread of iron in FG larger than the metallicity dispersion in M 54 (NGC 6715), the massive GC in the core of the tidally disrupting dwarf spheroidal galaxy Sagittarius of which M 54 probably represents the nuclear star cluster (Siegel et al. 2007, Carretta et al. 2010).

¹ Notice that L22 provide for ω Cen a mere spread of 0.148 dex. This GC is then dropped from the sample in Legnardi et al. (2024), together with a few others GCs, due to its complexity

At a given absolute luminosity, the colour of the RGB has a negligible dependence on the stellar mass, hence on the age of the stellar population, at least for ages higher than a few Gyr (e.g., Salaris, Cassisi, Weiss 2002). On the other hand, the position of a star across the RGB is strongly affected by the value of the metallicity. By comparing the colour spreads of the RGBs of the old stellar populations in the systems discussed above, one can grasp an immediate quantitative idea on the soundness and ranking of the different estimates. This comparison is done in Fig. 3, using for simplicity the Gaia bandpasses to overcome problems related to the variety of photometric systems used for GCs and dwarfs. Metal rich stars would be located on the red side of the RGB, whereas metal-poor stars would populate the bluer region, regardless of the selected bandpass.

To obtain the best sample of stars in NGC 5024, we considered the photometric constraints described in Leitinger et al. (2023). They use the UBVRI photometry by Stetson et al. (2019) and the resulting sample of stars was then cross-matched with the database of H. Baumgardt² of member stars in GCs. Red points in Fig. 3 are stars in NGC 5024 with membership probability ≥ 0.9 . Arbitrary shifts in colour $G_{BP}-G_{RP}$ and in G_{mag} were applied to make the RGB tip approximately coincide for all the compared systems, as we were simply interested in comparing the size of spread in colour as proxy of the metallicity spread.

We took the metallicity information for the dSph's Leo I and Fornax from Kirby et al. (2010), who used Keck/DEIMOS medium-resolution spectroscopy combined with spectral synthesis to derive them. That catalogue was cross-matched to Gaia data release 3 (GDR3, Gaia Collaboration et al. 2023) to obtain the magnitudes in the Gaia bandpasses for direct comparison with the GC CMDs. The sample of GC stars in ω Cen (NGC 5139) and NGC 6715 (M54) are from Stetson et al. (2019) and have also been cross-matched with GDR3.

The [Fe/H] spread in FG stars for NGC 5024 from L22 (0.307 dex) is slightly larger than the value reported by Willman and Strader (2012) for Fornax that, unlike GCs, is known to have experienced extended star formation lasting several Gyrs, as demonstrated from the width of the metallicity distributions and the age spreads deduced from its broadband colours (combined with spectroscopic metal abundances, e.g., Battaglia et al. 2006).

In the CMD of NGC 5024, stars on the asymptotic giant branch are well recognisable, and the stars unambiguously on the RGB form a very narrow sequence, as expected for a stellar population with the same age and composition, whereas old populations on the RGB of dSphs show a much larger spread in colour, more consistent with measured spectroscopic spreads of [Fe/H] of about 0.3 dex (Kirby et al. 2010, Willman and Strader 2012). The luminosity-Z spread relation observed in dSphs (e.g., Kirby et al. 2011) shows that dSphs were able to sustain a star formation of long duration thanks to the ability to retain the gas, the more effectively the more luminous is the galaxy. Conversely, the formation of GCs was an extremely fast event: none of the proposed scenarios (e.g., Bastian and Lardo 2018, Gratton et al. 2019) involves star formation his-

ories lasting more than a few tens of Myr, after which only passive evolution sets on. This time limit is established relying on the evolving times of various plausible candidates proposed for the enrichment in light, proton-capture elements characterising the MPs in GCs and the simultaneous lack of variations in heavier elements in most GCs.

Also instructive is the comparison shown in the lower two panels of Fig. 3, where NGC 5024 is plotted against the RGB colour distribution of the two most massive GCs in the Galaxy: ω Cen and M 54. Both GCs have an intrinsic [Fe/H] spread, well documented from spectroscopic or photometric measurements, and both are considered to be former nuclear star clusters of dwarf galaxies (e.g., Bekki and Freeman 2003, Carretta et al. 2010, see also the review by Gratton et al. 2004). Again, the spread in NGC 5024 estimated for FG stars by L22 seems to be completely at odds with the large values measured in the two massive GCs, as the comparison of the CMDs unambiguously shows (see also Fig. 1).

Typical uncertainties in magnitudes and colours are indicated by the error bars in Fig. 3, estimated from Table 3 of Gaia Collaboration et al. (2018a) and figure A.7 of Gaia Collaboration et al. (2018b). While the faint end of RGB in the more distant dwarf galaxies is close to the limits of precise Gaia photometry, the comparison at the bright regime does not support a correspondence between colour spreads and metallicity dispersions derived by L22. This is even more evident when the comparison involves NGC 5024 and other GCs like ω Cen and M 54³.

Beside this direct comparison of observables on the RGB, there is also support from theory to suggest that the metallicity spreads given in L22 are probably overestimated and unrealistic. The proto globular cluster clouds out of which ω Cen and M 54 formed were massive enough to satisfy the theoretical prerequisites for showing clear evidence of self-enrichment. These requirements are well illustrated by Dopita and Smith (1986) and include primary star formation with SN explosions and a potential well deep enough to trap the ejecta that must be able to cool enough to be used later in the following phase of secondary star formation.

For star formation to occur in gas enriched by SNe exploded in the primary star formation, the ejecta must cool and remain trapped in a layer of gas both gravitationally bound to the cloud and able to becoming self-gravitationally unstable. These constraints imply that there is a limit in mass for the progenitor of GCs to sustain some self-enrichment. Dopita and Smith (1986) calculated that energetic SN ejecta can be slowed below the escape velocity of the cloud, by explosions close to the mass center, only in clouds more massive than $\sim 3 \times 10^6 M_{\odot}$. Explosions near the tidal radius would have gas and metal enriched ejecta unavoidably lost to the intergalactic medium. At the low extreme, clouds would be completely disrupted by SN explosions if less massive than $\sim 10^5 M_{\odot}$. The bottom line is that only the most massive clouds are destined to form the final, self-enriched GCs.

³ The error bars close the the lower RGB region in the dwarf galaxies, when properly focused deep photometry is used, decrease to values more comparable to those of GCs.

² <https://people.smp.uq.edu.au/HolgerBaumgardt/globular/parameter.html>

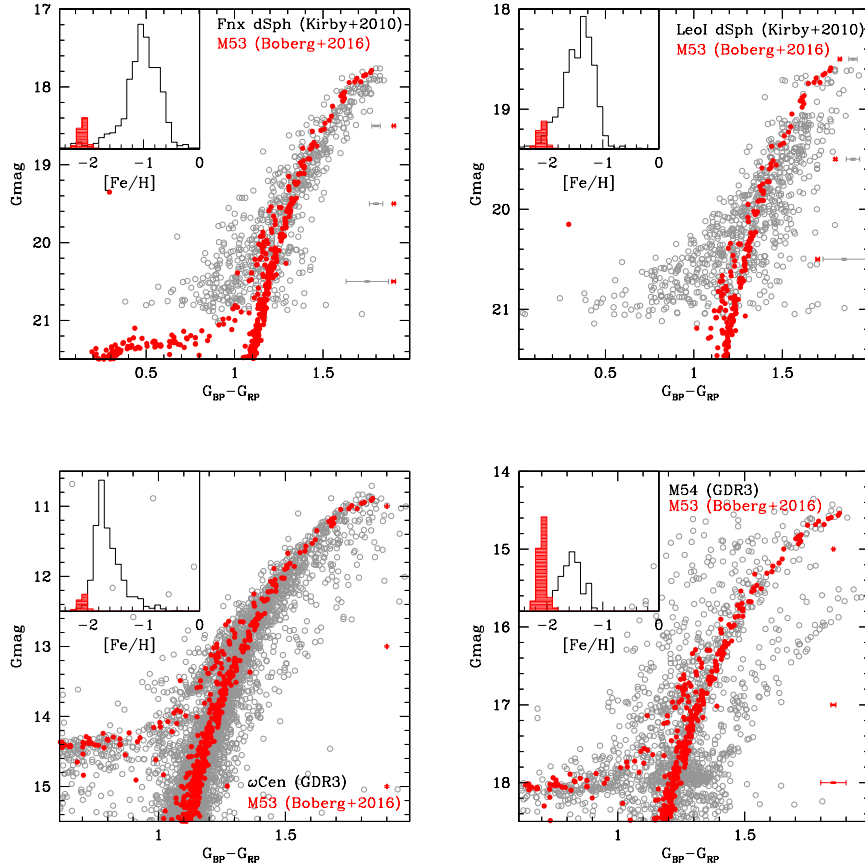


Fig. 3. Comparison of the RGBs in the CMDs of GCs and dwarf galaxies. Upper panels: NGC 5024 (M 53, filled red points) is compared to the dwarf galaxies Fornax and Leo I (empty circles). Lower panels: Comparison of NGC 5024 with two massive GCs, ω Cen and M 54 (left and right panel, respectively). The inset in each panel shows the metallicity distribution of the compared samples. Typical error bars in the Gaia photometric system are indicated.

A quantitative idea of the fraction of Galactic GCs potentially capable of satisfying these requisites is given in Fig. 4. The estimates of initial masses for the population of GCs in the Milky Way (Baumgardt et al. 2019) are plotted as a function of the present day masses (represented by the total absolute magnitude). The solid line shows the lower mass limit for a proto cluster cloud to efficiently retain SN ejecta according to the calculations by Dopita and Smith (1986). Only three GCs (namely ω Cen, M 54, and Liller 1) are expected to be above this threshold. NGC 5024 (red filled circle) lies well below the required value, even at the estimated beginning of its evolution, before its mass is next reduced by dynamical evolutionary effects (both internal and external).

We know, of course, that actually a number of GCs present traces of pollution by SNe, in various amounts. These are the GCs named iron complex clusters by Johnson et al. (2015): M 2, NGC 1851, M 54, ω Cen, NGC 5286, NGC 5824, NGC 6273, Terzan 5, M 22. A recent addition to this group is Liller 1 (Fanelli et al. 2024). The iron complex GCs are indicated in Fig. 4 as filled blue points and the dashed line (at about $9 \times 10^5 M_{\odot}$) defines the lower envelope for initial masses of these massive GCs. NGC 5024 lies just below the group of iron complex GCs, but allowing for uncertainties in the es-

timates of the initial masses of objects just slightly younger than the Universe, it could even match this less stringent constraint. However, the striking difference in $[\text{Fe}/\text{H}]$ spread between NGC 5024 and GCs with a spectroscopic spread of 0.3 dex still lingers. Boberg et al. (2016) find a dispersion of only 0.07 dex associated to the mean metallicity of NGC 5024 from a large sample of stars. This value is more similar to the one detected for NGC 1851 (Carretta et al. 2011b), a member of the iron complex GCs with a minimal inhomogeneity in $[\text{Fe}/\text{H}]$.

The conclusion from the present section is that the metallicity spread for FG in NGC 5024 (as well as for NGC 5272) computed by L22 from the PCM seems to be largely overestimated. Neither simple observations based on the comparison of the RGB colour spreads nor theoretical model constraints seem to support the notion of iron spread so large as advocated by L22 for these two GCs. Since the method used for NGC 5024 and NGC 5272 is not different from the one applied to the other GCs, a logical inference is that probably the estimates for the $[\text{Fe}/\text{H}]$ spread in FG stars of all GCs may be an overestimate.

These greatly overstated values derived from the PCMs could probably explain the discrepancies between high resolution spectroscopy and HST photometry, probed in the next Section.

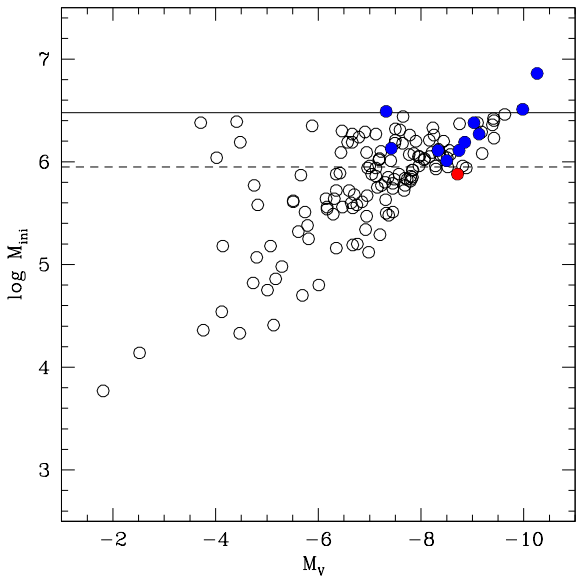


Fig. 4. Initial masses of GCs from Baumgardt et al. (2019) for the population of GCs in the Milky Way plotted as a function of the present-day total absolute luminosity. Solid and dashed lines indicate values $\sim 3 \times 10^6 M_{\odot}$ and $9 \times 10^5 M_{\odot}$. The red filled circle represents NGC 5024 and blue circles indicate GCs presently known to have in some extent a metallicity dispersion.

3. Discrepancies between spectroscopy and HST photometry

The approach used by L22 to derive a putative metallicity spread among FG stars is to link the extension of *RG1* to the width $W1g$ of FG stars on the RGB in the CMD m_{F814W} versus col taken from M17. The underlying principle is that stars of different metallicity occupy different sides of the RGB.

From Section 2 what does not compute is the sheer (and unbelievably large) amount of the spreads attributed to FG stars, derived by L22 by translating $W1g$ into metallicity. This was done using a generic “colour-metallicity relation” from Dotter et al. (2008). If the method used by L22 is the equivalent of interpolating mean ridge lines of GCs at different metallicities, but instead simply employing theoretical isochrones, it is susceptible to even larger errors. Salaris et al. (2002) stated that at fixed magnitude on the RGB a colour difference in $V - I$ of about 0.05 or 0.10 mag translates into uncertainties as large as $\sim 0.3 - 0.5$ dex when $[Fe/H]$ is determined from the comparison of observed and theoretical RGBs.

For the first time it is possible to test this scenario and obtain a more sound estimate of the variation in $[Fe/H]$ among FG stars thanks to the large (and unique, so far) published database of stars used for the chemical tagging of the PCMs in CB24. From the few hundreds stars with both HST photometry and high resolution spectroscopy identified in 22 GCs, we considered 159 FG stars. These stars lie on the *RG1* and are classified as FG with spectroscopy, according to their Na abundance, since we showed that a number of stars tagged using photometric criteria are actually mismatches, that is FG stars misclassi-

fied as SG stars and vice versa (CB24). We prefer to rely on the criterion based on Na, since the abundance from spectroscopy is the direct discriminant for MPs in GCs (see Carretta et al. 2009b).

A popular technique to investigate possible metallicity spreads among FG stars is the so called differential abundance analysis of stars with nearly identical atmospheric parameters, since it permits to have very small uncertainties associated to the derived abundances (see e.g., Lardo et al. 2023). The precise abundances can be then related to the position of stars along *RG1*.

To have a better insight on the true link between the extension of *RG1* and iron spread we applied a similar method starting with the above large sample of 159 FG stars. We further culled the sample by rejecting the stars found to be misclassified as FG by photometry (CB24). Additionally, we excluded four other stars classified as SG from their Na abundances and not recognized in CB24. Furthermore, eight stars were conservatively rejected due to their uncertain position between *RG1* and *RG2*. In each GC we then searched and paired stars with similar atmospheric parameters. Finally, we ended up with 46 genuine FG stars in 12 GCs. We combined these stars in 30 pairs with a maximum difference in effective temperature of 32 K (on average the difference in T_{eff} is -4.6 K, $\text{rms}=16$ K). The pairs are listed in Table 2. For each paired up star we report the identification of the pair, the position in the *RG1* of the PCM, the values of $[Fe/H]$ and $[Na/Fe]$, the star ID from Nardiello et al. (2018), where the stellar coordinates can be found, the name of the GC with its average metallicity, and the atmospheric parameters effective temperature, surface gravity, model abundance $[A/H]$, and microturbulent velocity. References for the abundance analysis are given in the last column. Most of the analysis are from our homogeneous FLAMES survey (see Carretta et al. 2006), except for NGC 6121, for which we used an independent source (Marino et al. 2008) as a safety check.

The similarity of atmospheric parameters means that comparing the stars in each couple we are doing an extensive differential analysis. If there is any metallicity spread in any given GC, the assembled dataset of stars with nearly identical parameters should reveal a correlation between $[Fe/H]$ and position along the Δcol in *RG1*.

The results of this exercise are plotted in Fig. 5 and Fig. 6. On top of each panel we report the GC name, the absolute value of the metallicity difference of the two stars (the order of the stars in each pair is not relevant) and their absolute difference along the Δcol coordinate in the *RG1* of the PCM (we are interested only in mapping the distance between the stars). Moreover, the metallicities of the stars are labelled at the bottom of each panel. The $[Fe/H]$ value of the star with the bluer Δcol value is always put on the left and the value for the redder Δcol star on the right. Stars with very similar parameters may be used to form more than a single pair.

The first clear evidence from these figures is that the star at bluer Δcol is not always the most metal-poor (pairs 2, 5, 7, 11, 13, 14, 19, 21, 23, 24, 25, 29). In these cases, the bluer position is occupied by the more metal-rich star in the couple, albeit sometime by tiny amounts in $[Fe/H]$.

Table 2. Pairs of FG stars with similar atmospheric parameters

pair	Δcol	$\Delta col3$	[Fe/H]	[Na/Fe]	ID	GC	[Fe/H] _{GC}	Atm.parameters	ref. abundance analysis
1	-0.0591	0.0218	-1.240	0.017	R0000202	288	-1.219	5073 2.69 -1.24 1.13	Carretta et al. (2009b)
1	-0.0477	0.0725	-1.188	-0.002	R0001020	288	-1.219	5103 2.68 -1.18 1.09	
2	-0.0690	0.0064	-1.150	0.065	R0006958	2808	-1.128	4493 1.54 -1.15 1.52	Carretta (2015)
2	-0.1760	0.0671	-1.111	0.078	R0035565	2808	-1.128	4461 1.45 -1.11 1.50	
3	-0.0690	0.0064	-1.150	0.065	R0006958	2808	-1.128	4493 1.54 -1.15 1.52	
3	-0.1844	0.0337	-1.161	-0.032	R0038704	2808	-1.128	4502 1.52 -1.16 1.56	
4	-0.0852	-0.0153	-1.113	-0.082	R0037787	2808	-1.128	4703 1.89 -1.11 1.35	
4	-0.2384	0.0431	-1.168	-0.089	R0039175	2808	-1.128	4712 1.88 -1.17 1.54	
5	0.0954	-0.0221	-1.457	-0.103	R0000657	3201	-1.495	4737 2.17 -1.46 1.67	Carretta et al. (2009b)
5	-0.0927	0.0098	-1.432	-0.196	R0000897	3201	-1.495	4733 2.18 -1.43 1.11	
6	0.0954	-0.0221	-1.457	-0.103	R0000657	3201	-1.495	4737 2.17 -1.46 1.67	
6	-0.4515	0.1263	-1.562	-0.122	R0002678	3201	-1.495	4761 2.26 -1.57 1.42	
7	0.0270	0.0140	-1.496	-0.246	R0000690	3201	-1.512	4495 1.61 -1.50 1.59	
7	0.0105	-0.0009	-1.440	-0.129	R0001697	3201	-1.512	4496 1.61 -1.44 1.69	
8	-0.4515	0.1263	-1.562	-0.122	R0002678	3201	-1.495	4761 2.26 -1.57 1.42	
8	-0.0927	0.0098	-1.432	-0.196	R0000897	3201	-1.495	4733 2.18 -1.43 1.11	
9	-0.0221	0.0164	-2.265	0.036	R0000883	4590	-2.227	4856 2.01 -2.26 0.41	Carretta et al. (2009b)
9	-0.0522	0.0234	-2.304	0.009	R0001662	4590	-2.227	4833 2.01 -2.30 0.20	
10	0.0054	-0.0531	-2.019	0.022	R0004864	4833	-2.040	4829 2.05 -2.02 1.68	Carretta et al. (2014)
10	-0.0489	-0.0006	-2.038	0.031	R0003934	4833	-2.040	4852 2.09 -2.04 1.59	
11	-0.1730	0.1328	-1.813	0.125	R0012060	6093	-1.792	4414 1.18 -1.81 1.39	Carretta et al. (2015)
11	-0.1604	0.1297	-1.843	0.177	R0012523	6093	-1.791	4434 1.21 -1.84 1.58	
12	-0.1331	0.0233	-1.804	0.038	R0004959	6093	-1.791	4935 2.23 -1.80 1.54	
12	-0.0828	0.1008	-1.791	0.225	R0003113	6093	-1.791	4952 2.25 -1.79 1.23	
13	-0.0722	0.0217	-1.784	0.170	R0002307	6093	-1.791	5056 2.46 -1.78 0.65	
13	-0.1606	0.1118	-1.782	0.030	R0012580	6093	-1.791	5065 2.48 -1.78 1.82	
14	-0.0764	0.0798	-1.763	0.154	R0003844	6093	-1.791	5111 2.58 -1.76 0.67	
14	-0.0642	0.0636	-1.772	-0.020	R0001255	6093	-1.791	5111 2.56 -1.77 1.96	
15	-0.0642	0.0636	-1.772	-0.020	R0001255	6093	-1.791	5111 2.56 -1.77 1.96	
15	-0.0932	0.1011	-1.796	0.169	R0010817	6093	-1.791	5117 2.59 -1.80 1.75	
16	-0.0746	-0.0104	-1.446	-0.043	R0001634	6254	-1.556	4938 2.37 -1.44 0.82	Carretta et al. (2009b)
16	-0.1384	0.0208	-1.640	-0.137	R0001704	6254	-1.556	4932 2.35 -1.64 1.12	
17	0.0578	0.0203	-1.549	-0.128	R0001056	6254	-1.556	5011 2.50 -1.55 1.27	
17	-0.1435	0.0441	-1.577	-0.117	R0004888	6254	-1.556	5014 2.52 -1.58 1.85	
18	-0.1435	0.0441	-1.577	-0.117	R0004888	6254	-1.556	5014 2.52 -1.58 1.85	
18	-0.0438	-0.0074	-1.466	-0.096	R0001523	6254	-1.556	5032 2.55 -1.47 1.54	
19	-0.0001	0.0004	-2.058	-0.001	R0000841	6397	-1.993	4931 2.42 -2.06 0.35	Carretta et al. (2009b)
19	-0.0252	0.0128	-2.036	-0.153	R0000943	6397	-1.993	4936 2.05 -2.04 1.38	
20	-0.0427	0.0153	-1.880	-0.170	R0000162	6535	-1.963	4901 2.58 -1.88 0.80	Bragaglia et al. (2017)
20	-0.0720	0.0164	-1.950	-0.059	R0000450	6535	-1.963	4886 2.55 -1.95 0.83	
21	-0.0427	0.0153	-1.880	-0.170	R0000162	6535	-1.963	4901 2.58 -1.88 0.80	
21	-0.0186	-0.0049	-1.970	-0.017	R0000199	6535	-1.963	4926 2.29 -1.97 1.39	
22	-0.0829	0.0260	-1.611	0.050	R0006086	6752	-1.555	4315 1.12 -1.61 1.50	Carretta et al. (2009c)
22	-0.0806	0.0520	-1.548	0.126	R0003489	6752	-1.555	4338 1.19 -1.55 1.66	
23	-0.1417	0.0232	-0.773	0.113	R0000776	6838	-0.808	4777 2.48 -0.77 1.49	Carretta et al. (2009b)
23	-0.0796	0.0483	-0.862	0.233	R0001634	6838	-0.808	4766 2.47 -0.86 1.07	
24	-0.1417	0.0232	-0.773	0.113	R0000776	6838	-0.808	4777 2.48 -0.77 1.49	
24	-0.0687	0.0240	-0.776	0.137	R0001344	6838	-0.808	4785 2.49 -0.78 1.62	
25	-0.0687	0.0240	-0.776	0.137	R0001344	6838	-0.808	4785 2.49 -0.78 1.62	
25	-0.0578	0.0060	-0.787	0.233	R0000187	6838	-0.808	4800 2.47 -0.79 1.37	
26	-0.0578	0.0060	-0.787	0.233	R0000187	6838	-0.808	4800 2.47 -0.79 1.37	
26	-0.0978	0.0353	-0.837	0.240	R0000458	6838	-0.808	4814 2.51 -0.84 1.39	
27	-0.1979	0.0756	-1.070	0.00	R0000591	6121	-1.070	4800 2.47 -1.07 1.37	Marino et al. (2008)
27	-0.0997	0.0496	-1.050	0.00	R0002084	6121	-1.070	4800 2.57 -1.05 1.18	
28	0.0676	0.0119	-1.000	0.06	R0000301	6121	-1.070	4830 2.56 -1.00 1.25	
28	-0.0470	0.0434	-1.090	0.13	R0000346	6121	-1.070	4830 2.52 -1.09 1.28	
29	-0.0470	0.0434	-1.090	0.13	R0000346	6121	-1.070	4830 2.52 -1.09 1.28	
29	-0.0618	-0.0084	-1.080	0.07	R0001488	6121	-1.070	4850 2.54 -1.08 1.34	
30	-0.0618	-0.0084	-1.080	0.07	R0001488	6121	-1.070	4850 2.54 -1.08 1.34	
30	-0.1268	0.0543	-1.090	0.02	R0001736	6121	-1.070	4850 2.63 -1.09 1.22	

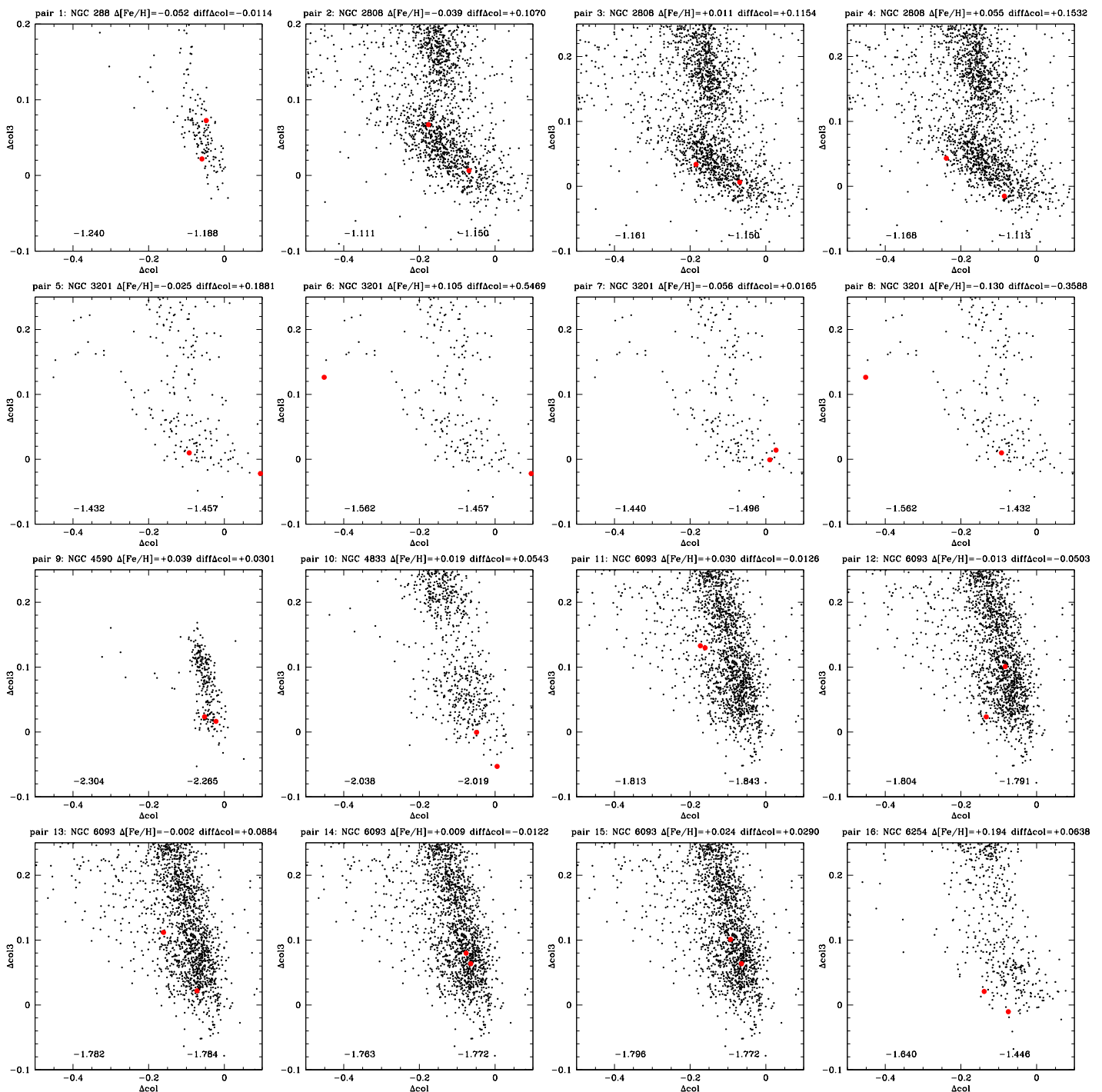


Fig. 5. Position of pairs of FG stars with similar atmospheric parameters (large red filled symbols) in NGC 288, NGC 2808, NGC 3201, NGC 4590, NGC 4833, NGC 6093, and NGC 6254

Second, stars at the same (or very similar) position in $RG1$ have noticeably distinct $[Fe/H]$ values (pairs 1, 7, 9, 11, 15, 19, 20, 21, 22, 25). Vice versa, in some other cases small amounts of difference in $[Fe/H]$ (from 0.01 to less than 0.05 dex) correspond to large distance in Δcol (pairs 2, 3, 4, 5, 12, 13, 17, 27, 30).

The relation between the displacement in $[Fe/H]$ and in Δcol is summarised in Fig. 7. As could be inferred from the above discussion, there is no correlation or proportionality be-

tween these quantities. Over 30 pairs of stars the mean value of the shift in Δcol is 0.090 mag (rms=0.114 mag). To this nearly constant shift does correspond a large range in metallicities, up to 0.2 dex, between stars in pairs, although the average difference in $[Fe/H]$ is not significant (0.049 dex, rms=0.045 dex).

Only in NGC 3201 large differences in $[Fe/H]$ seem to be matched by large differences along the length of the $RG1$. Even in this GC, however, the apparent correlation is not statistically significant (two-tails probability $p=0.32$, 4 data points).

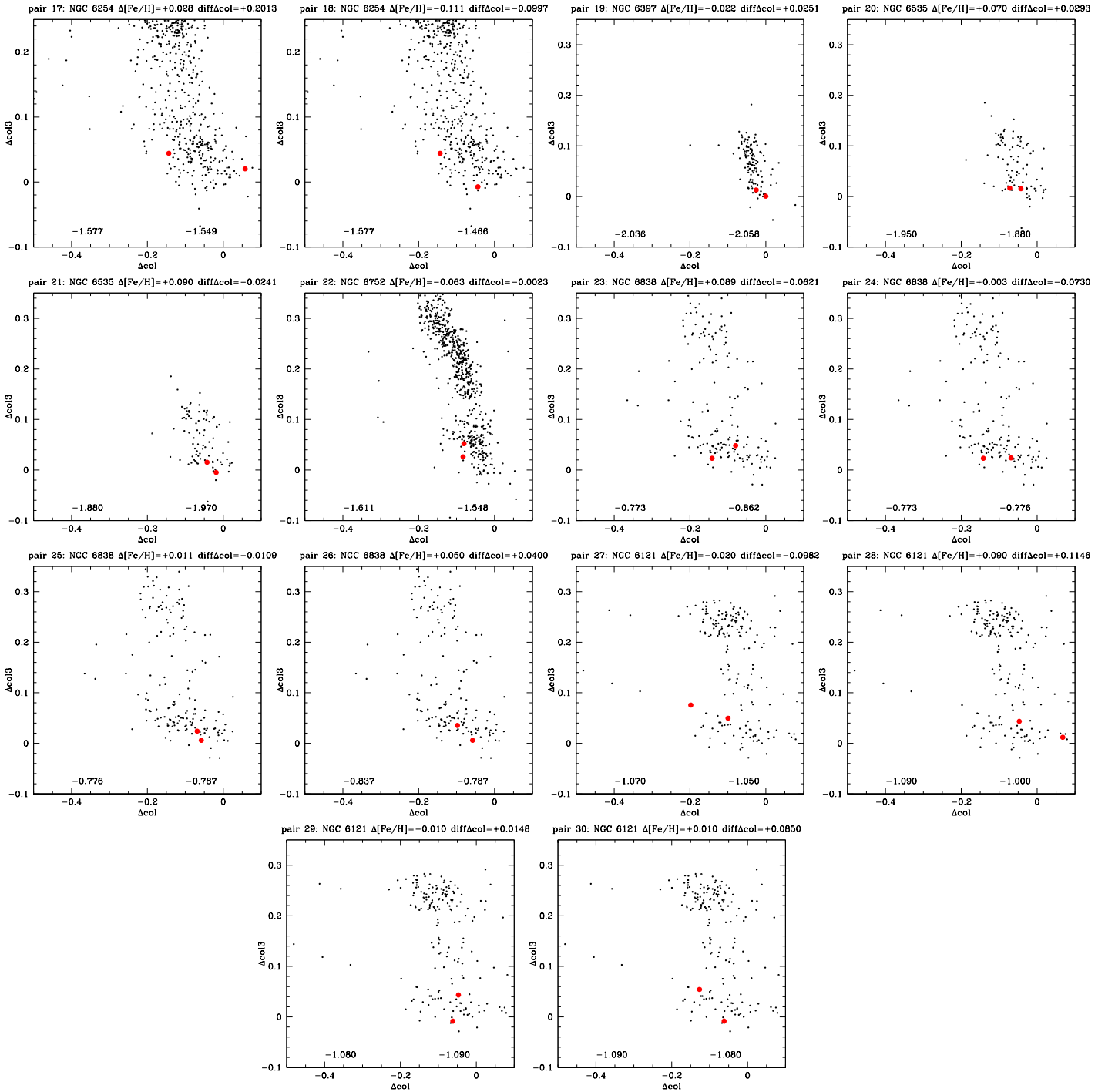


Fig. 6. Position of pairs of FG stars with similar atmospheric parameters (red circles) in NGC 6254, NGC 6397, NGC 6535, NGC 6838, and NGC 6121.

On the other hand, from Fig. 5 and Fig. 6 it is clear that most of the extended *RG1* sequence in NGC 2808 is explained by couple of stars with differences in $[\text{Fe}/\text{H}]$ of 0.04, 0.01, and 0.05 dex only (pairs 2,3,4, at odds with the results by Lardo et al. 2023), whereas L22 claim an unlikely large iron spread of 0.110 dex to explain the length of *RG1* in this GC.

The conclusion from these extensive differential analysis is that there seems to be no simple or direct correspondence

between metallicity spread and extension of the *RG1* region in the PCMs.

4. Quantifying the extension of the *RG1* sequences in the PCM

Despite the results from the previous Section, a different location of stars in Δcol on the *RG1* in the PCMs according to the metallicity of the star should be expected. The colour

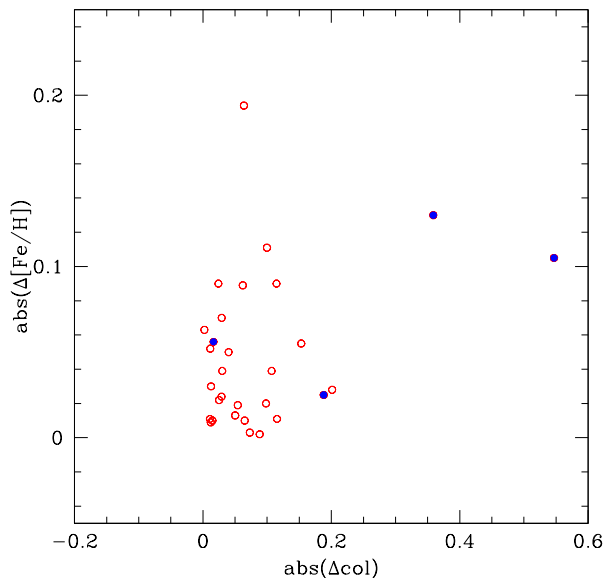


Fig. 7. Summary of the variations of $[\text{Fe}/\text{H}]$ as a function of the Δcol variation along the $RG1$ region on the PCM from 30 pairs of FG stars with similar atmospheric parameters. The plotted values are the absolute differences in $[\text{Fe}/\text{H}]$ and Δcol between the two stars in each pair. Pairs formed with stars in NGC 3201 are plotted as filled blue circles.

$\text{col} = m_{F275W} - m_{F814W}$ (and, differentially, the pseudo-colour Δcol) with its long baseline is sensitive mostly to the effective temperature of stars (see e.g., CB24). Hence the spread in Δcol suggested the inference made by M17 and L22 of a metallicity spread, since the He content of a FG star is the one established by the Big Bang nucleosynthesis, by definition.

For a given age, metal-poor stars are located on the blue side of the RGB in the CMD, metal rich stars lie on the red side. In the same way, also when building a PCM stars with lower metallicity are expected at bluer (more negative) Δcol values whereas metal rich stars can be expected to be at redder (less negative) values of Δcol along $RG1$. However, neither L22 nor M17 provide a precise quantity to express what they mean with the statement that the extension of $RG1$ is too large with respect to the errors. No precise measurements of this extent are given or published.

We fix this shortcoming by providing for the first time the extension of $RG1$ in the PCMs of the GCs published in CB24. To quantify the sequence $RG1$ we used three kind of indicators (see the sketch in Fig. 8): 1) the interquartile range iqrFG in Δcol of the FG stars, to minimize the uncertainties introduced by outliers; 2) the rms relative to the mean Δcol value of the FG stars, rmsFG ; and 3) the major axis of the ellipse that best encloses the $RG1$ sequence, lenRG1 .

More in detail, first we isolated FG and SG stars for each GC on the corresponding PCM. Conservatively, we dropped from the CB24 sample NGC 6388 and NGC 6715 whose uncertainties due to the high reddening and to field contamination may hamper somehow the results. The measurements for all the other 20 GCs are listed in Table 3.

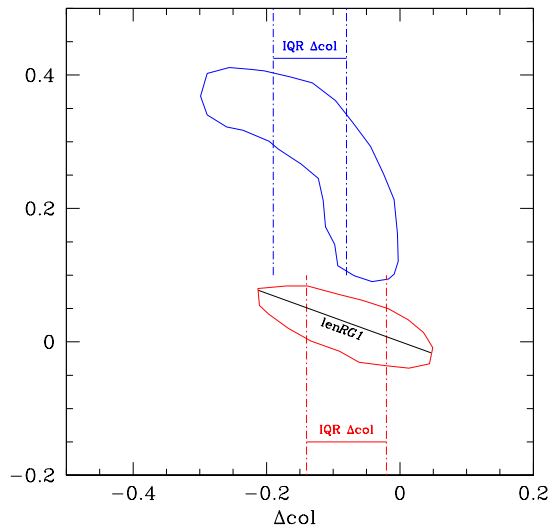


Fig. 8. Schematic plot of a PCM, with $RG1$ and $RG2$ indicated in red and blue, respectively. The lines and segments show the different measures of their extension in Δcol , and along the elongated region of FG stars enclosed by the ellipse (see text for a description).

Table 3. Extensions and spreads in Δcol for $RG1$ and $RG2$

GC	lenRG1	rmsFG	iqrFG	rmsSG	iqrSG	b/a	ang
104	0.290	0.056	0.079	0.054	0.071	0.60	34.99
288	0.142	0.061	0.037	0.023	0.029	0.50	50.00
362	0.160	0.034	0.041	0.047	0.056	0.50	28.96
1851	0.186	0.038	0.049	0.048	0.059	0.50	30.00
2808	0.394	0.079	0.098	0.113	0.175	0.35	16.38
3201	0.356	0.084	0.103	0.062	0.090	0.30	15.67
4590	0.084	0.020	0.023	0.019	0.026	0.35	20.00
4833	0.244	0.053	0.065	0.042	0.058	0.60	25.00
5904	0.206	0.047	0.053	0.046	0.062	0.35	30.00
6093	0.222	0.045	0.053	0.050	0.067	0.70	20.00
6121	0.246	0.073	0.097	0.056	0.064	0.30	7.51
6205	0.166	0.036	0.043	0.051	0.074	0.55	18.93
6254	0.286	0.063	0.077	0.044	0.061	0.45	28.00
6397	0.058	0.026	0.025	0.015	0.020	0.50	30.02
6535	0.120	0.034	0.052	0.036	0.051	0.55	19.99
6752	0.138	0.034	0.035	0.039	0.060	0.75	30.00
6809	0.084	0.020	0.033	0.023	0.032	0.70	40.00
6838	0.300	0.062	0.095	0.057	0.080	0.40	20.00
7078	0.230	0.047	0.063	0.056	0.059	0.30	9.49
7099	0.088	0.021	0.027	0.026	0.036	0.50	20.00

The selection of stars to be assigned to $RG1$ and $RG2$ is made interactively using TOPCAT (Taylor 2005); for most cases the selection, simply done visually, is straightforward, while in other cases there is some ambiguity. This is true also for the PCMs computed by M17, as clearly shown in their plots. We verified that these groups are properly located in the $m_{F814W} - \text{col}$ and $m_{F814W} - \text{col3}$ CMD in the position where FG and SG stars lie. Our selection is shown for all GCs in the figures in Appendix A, where FG and SG stars are plotted in red

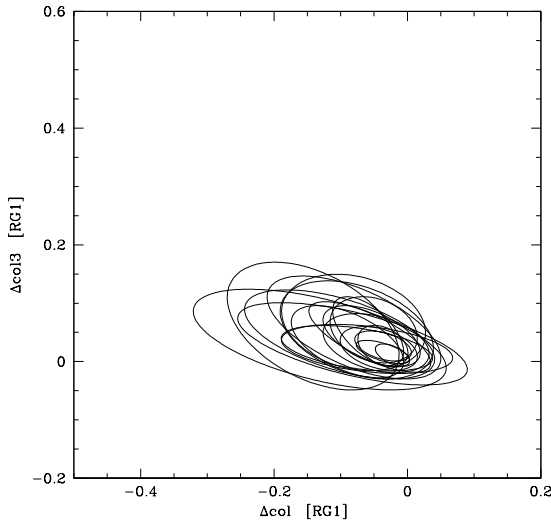


Fig. 9. Ellipses representing the *RG1* region in all GCs considered here. The major axis length, the axis ratio, and the inclination were derived as described in the text.

and blue, respectively, whereas stars with an uncertain attribution are in grey. Stars in this latter group are always a minority. In the worst case (NGC 2808) they are less than 15% and they do not alter our results, being clearly located slightly outside the tight sequences of the RGB.

Once we have the samples of FG stars, we do a linear interpolation so we can measure the inclination of the FG distribution in the PCM. This is also the inclination of the ellipse that best encloses the FG stars, apart from a few slight adjustments made by eye. The values of the position angles are measured clockwise starting from the x-axis of the PCM and listed in Table 3.

The orientation of the *RG1* region is similar, but not equal among GCs (see Fig. 9). This is in contrast with the procedure by M17, who adopted a line with a fixed inclination (an angle of 18 degrees with respect to the x-axis in the PCM) to separate FG and SG stars. Although the average inclination in our sample of GCs (24.75 degrees, with an rms=10.11) seems not very different from the value used by M17, the individual *RG1* span a range from the 7 degrees in NGC 6121 up to the steep 50 degrees of the FG stars in NGC 288.

All the derived indicators *iqrFG*, *rmsFG*, and *lenRG1* are tightly correlated with each other, as shown in the upper part of Table 4 (correlations 1, 2, and 3), that is they measure essentially the same quantity and are equivalent as true estimates of the extension of *RG1* in the PCMs. In this table we list for each correlation the involved parameters, the Pearson's correlation coefficient for the linear regression and the two-tails probability testing the null hypothesis that the observed values come from a population in which the true correlation is zero. We also measured the extension in Δcol of the *RG2* sequence, again taking into consideration the interquartile range *iqrSG* and the *rmsSG* values. Due to the shape of the *RG2* regions, it was not

possible to use simple geometric forms like the ellipse to measure their extension, anyway both *iqrSG* and *rmsSG* are well suited to quantify the spread of SG stars in Δcol (correlation 4 in Table 4).

For geometric reasons we chose the major axis of the ellipse as our preferred observable for the extension of the *RG1* region since it reproduces the length of the FG distribution exactly along the direction where it is more elongated. Notice that L22 and M17 only used the displacement in Δcol along the horizontal axis, without considering the inclination of *RG1*. In other words, their measurements are a scaled version of our measured extensions according to the Pythagoras' theorem. We will use *lenRG1* to investigate the dependence of the *RG1* region on global GC parameters. On the other hand, to quantitatively compare the properties of FG and SG stars we are necessarily forced to employ the other quantities, *iqr* and *rms* values.

In most cases the values of *iqrFG* and *iqrSG* (as well as *rmsFG* and *rmsSG*) are not dramatically different. This result is unexpected, since it is generally claimed that the extension in Δcol is larger for FG than for SG stars (see e.g., L22 and M17). We note that the derivation of a metallicity spread in M17 and L22 is focused only on the FG spread or extension in Δcol , whereas the similar spread in SG stars is almost completely neglected, albeit it is significant (see next Section). The cluster NGC 2808 is the most extreme case, since its *lenRG1* is smaller than the extent of *RG2*. Excluding NGC 2808, the average values become more comparable, as shown by the *iqr* values in Table 3.

The relation of the measured extent of *RG1* with respect to other relevant quantities is shown in Fig. 10. Statistical values for the correlations (or the lack of any relation) regarding mutual parameters of the MPs in GCs are reported in the middle part of Table 4. Possible interesting correlations with global GC parameters have their statistical values listed in the third part of Table 4.

The first consideration from Fig. 10 (upper left panel) is that there is no correlation between the extent of the *RG1* sequence of FG stars and the values of the metallicity spread as computed by L22 (see correlation 12 in Tab. 4). This striking evidence is clearly visualised in Fig. 11. In the four panels of this figure we grouped GCs according to the [Fe/H] spread of FG stars derived by L22, and for each group we plotted the ellipses enclosing the *RG1* sequences. As a matter of fact, metallicity spreads and extensions of FG stars in the PCM are unrelated. Putative, almost identical FG [Fe/H] spreads correspond to wildly different extensions of *RG1*.

Similarly, there is no correlation between *lenRG1* and the fraction of FG stars in each GC estimated by M17 on the PCM (upper right panel in Fig. 10 and correlation 5 in Table 4). Thus, how much the *RG1* extends seems to be not dependent on the number of FG stars in the GC, apparently requiring the involvement of some other parameters.

A robust correlation does actually exist between the extension *lenRG1* and the width *W1g* of the FG stars on the RGB in $col = m_{F275W} - m_{F814W}$ from M17 (lower left panel in Fig. 10). This width is the same used by L22 as starting point to translate the width of the FG region into a metallicity spread. Hence, the

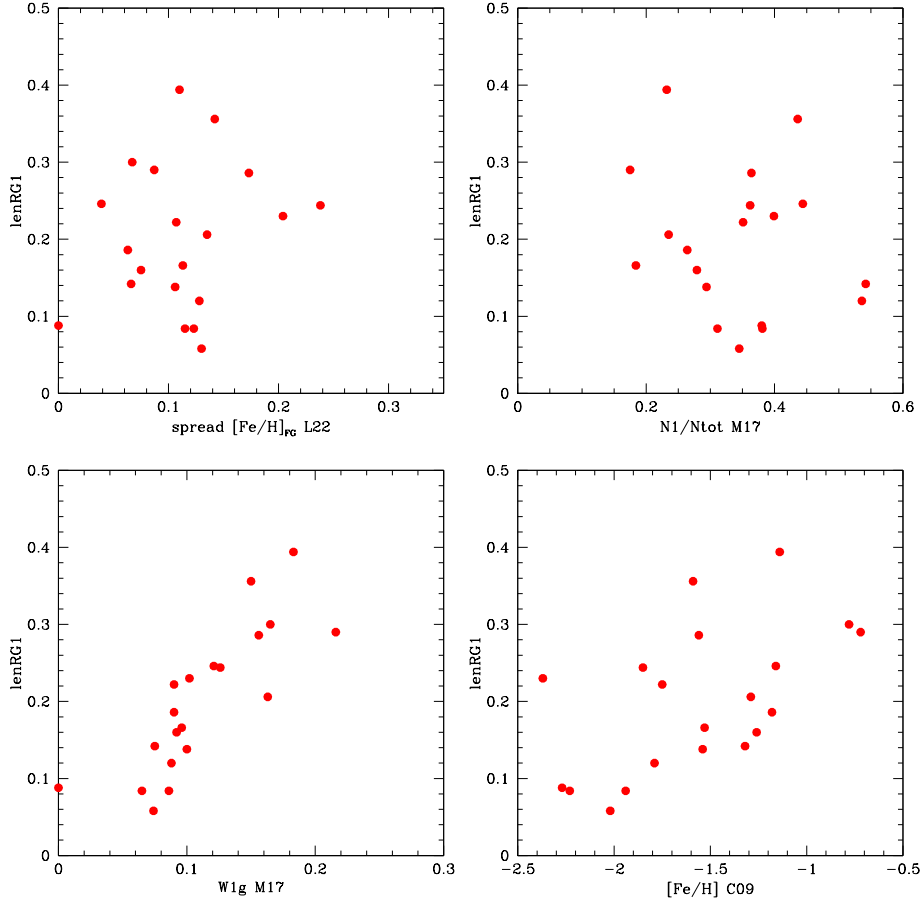


Fig. 10. Extension of the region *RG1* plotted with respect to other quantities. Upper left panel: Metallicity spread of FG stars by L22. Upper right panel: Fraction of FG stars in each GC from M17. Lower left panel: Width of the FG stars on the RGB in the $m_{F814W} - col$ CMD from M17. Lower right panel: Metallicity of GCs on the metallicity scale by Carretta et al. (2009a).

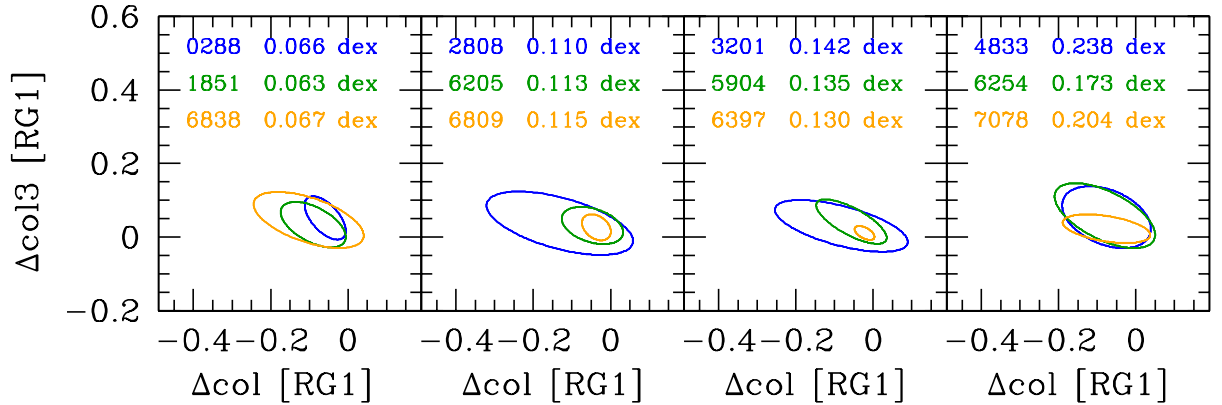


Fig. 11. Relation (or lack thereof) between the extension in *RG1* (here describer by the major axis of the ellipses) and the spread in metallicity proposed by L22. For clarity, we show four panels with only three cases with similar spreads, as claimed by L22, in each one. The GCs and the metallicity spreads are indicated in the plots with the same colour as the corresponding ellipse. The extensions $lenRG1$ are in Table 3.

results of correlations (6) and (12) altogether would suggest once more that the width $W1g$ of FG stars used by L22 are sound, being wider as the $lenRG1$ is larger, but are somehow converted into unrealistic metallicity spreads that, moreover, do not seem to have any correspondence with the measured

extension of *RG1* in the PCM. This would then suggest that it is the conversion of $W1g$ into $[Fe/H]$ values to be the source of the error.

Moreover, there is a positive and statistically significant correlation between the $lenRG1$ and the GC global metallic-

Table 4. Correlations of extensions and other parameters

Extensions				
corr.	parameters	r_P	prob.	data source
(1)	lenRG1 - rmsFG	+0.900	$< 1.0 \times 10^{-6}$	this work
(2)	lenRG1 - iqrFG	+0.934	$< 1.0 \times 10^{-6}$	this work
(3)	iqrFG - rmsFG	+0.907	$< 1.0 \times 10^{-6}$	this work
(4)	iqrSG - rmsSG	+0.976	$< 1.0 \times 10^{-6}$	this work
MP parameters				
corr.	parameters	r_P	prob.	data source other than this work
(5)	lenRG1 - N1/Ntot	-0.027	0.91	Milone et al. (2017)
(6)	lenRG1 - W1g	+0.815	1.2×10^{-5}	Milone et al. (2017)
(7)	lenRG1 - W2g	+0.621	3.5×10^{-3}	Milone et al. (2017)
(8)	W1g - W2g	+0.515	2.0×10^{-2}	Milone et al. (2017)
(9)	iqrSG - W1g	+0.638	2.5×10^{-3}	Milone et al. (2017)
(10)	iqrSG - W2g	+0.858	1.0×10^{-6}	Milone et al. (2017)
(11)	iqrSG - iqrFG	+0.719	3.5×10^{-4}	
GC parameters				
corr.	parameters	r_P	prob.	data source other than this work
(12)	lenRG1 - Fe spread	+0.205	0.39	L22
(13)	lenRG1 - [Fe/H]	+0.550	1.2×10^{-2}	Carretta et al. (2009a)
(14)	lenRG1 - σ_0	+0.043	0.86	Bailin and Von Klar (2022)
(15)	lenRG1 - σ_{Fe}	-0.111	0.64	Willman and Strader (2012)
(16)	lenRG1 - age	-0.349	0.13	Kruijssen et al. (2019)
(17)	lenRG1 - M_V	-0.341	0.14	Harris (2010)
(18)	lenRG1 - M_{ini}	+0.279	0.23	Baumgardt et al. (2019)
(19)	lenRG1 - iqr[O/Na]	+0.234	0.32	Carretta et al. (2010c)
(20)	iqrSG - [Fe/H]	+0.474	3.5×10^{-2}	Carretta et al. (2009a)
(21)	iqrSG - M_{ini}	+0.443	0.050	Baumgardt et al. (2019)
(22)	rmsSG - M_{ini}	+0.467	0.038	Baumgardt et al. (2019)

ity (lower right panel of Fig. 10), on the metallicity scale by Carretta et al. (2009a). However, this correlation goes in the opposite direction with respect to the one given by L22. In L22 larger metallicity spread are found for metal-poor GCs (see their Figure 12 or their Table 4), whereas in Fig. 10 the lenRG1 is larger in more metal-rich GCs.

Finally, lenRG1 does not correlate with the GC intrinsic metallicity spreads (correlations 14 and 15 in Table 4) or the age and mass (either present-day mass or initial mass) of the GCs (correlations 16, 17, and 18). Not significant is also the relation of lenRG1 with the extension of the Na-O anticorrelation, the main spectroscopic signature of MPs (correlation 19).

A maybe unexpected result when quantifying the extension of the sequences in the PCM is shown in Fig. 12. We found that the extension of RG1 is tightly correlated to the extent of the RG2 in Δcol . In this figure we also report the Pearson's correlation coefficient. The tight relation between iqrFG and iqrSG is true regardless NGC 2808 is included ($p = 3.5 \times 10^{-4}$) or not ($p = 5.9 \times 10^{-5}$) in the sample. This result prompted us to have a more careful look at the extension of the RG2 sequence and its relation to the global cluster parameters, filling the void left in the M17 and L22 analysis who only focus on the spread in Δcol of the FG stars.

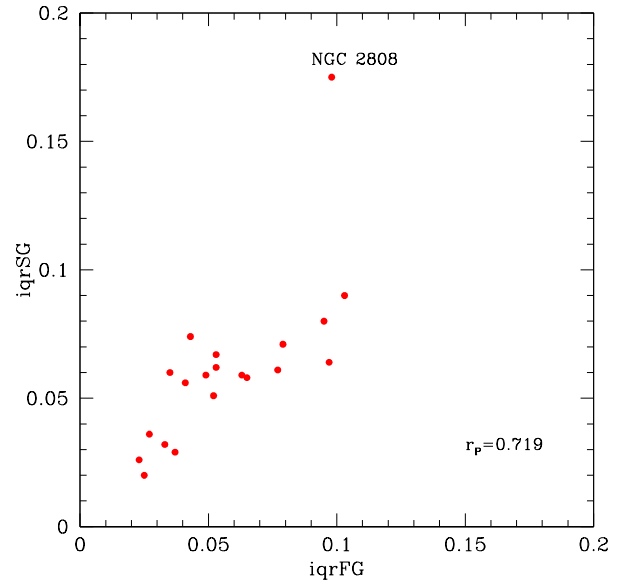


Fig. 12. The extension of the RG2 region as a function of the extension of the sequence of FG stars, RG1. The Pearson's correlation coefficient is reported.

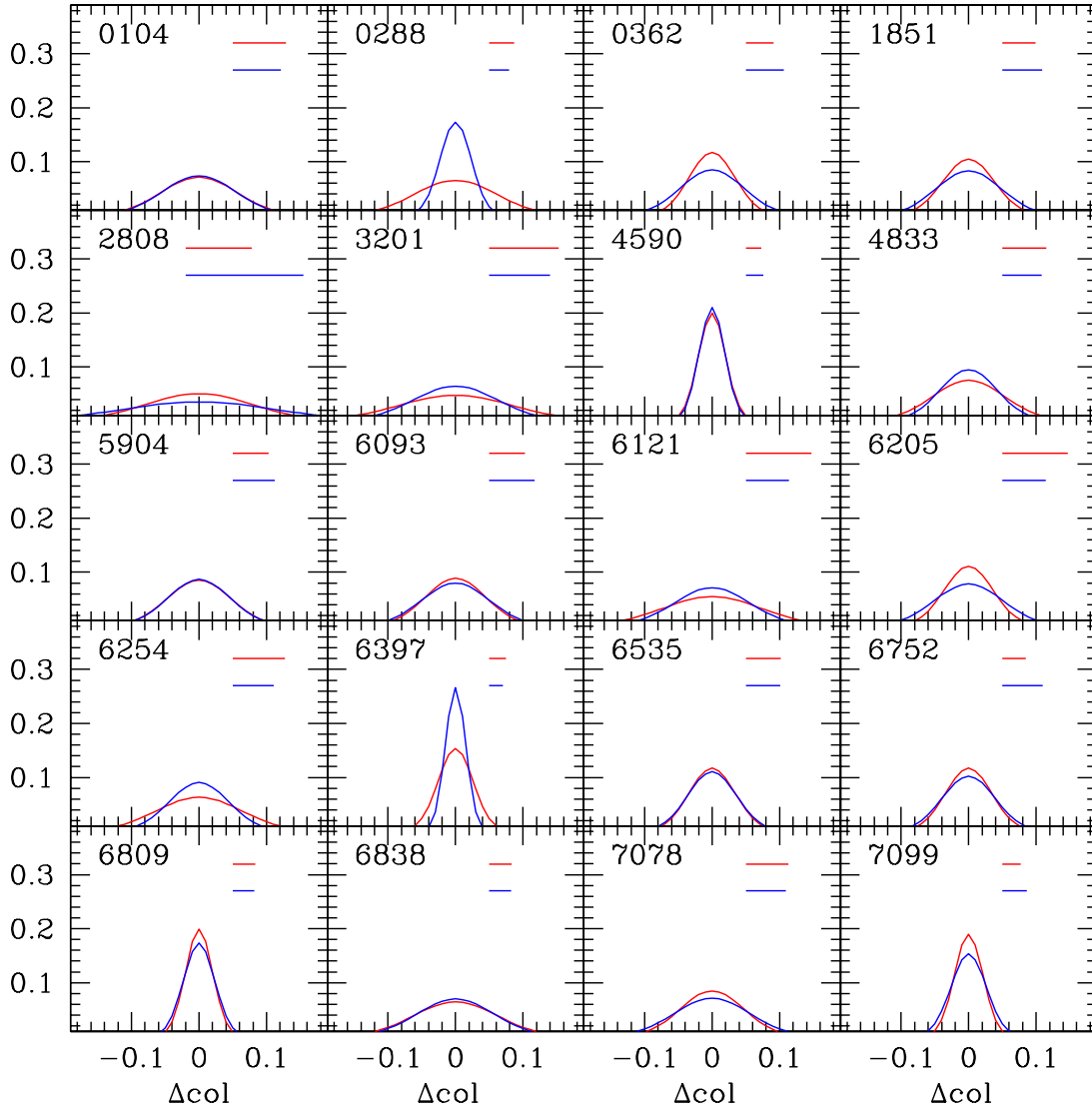


Fig. 13. Comparison between the distributions of *RG1* (in red) and *RG2* (in blue) in Δcol in 20 GCs from CB24. In each panel the two Gaussians with σ equal to the rms are shown. The peaks have been shifted both to zero to get an immediate comparison. The horizontal lines in each panel indicate the iqrFG and iqrSG (red and blue, respectively).

5. The elephant in the room: Spreads in the neglected SG stars in GCs

The basic observation upon which a claim of a metallicity spread is based is the large extension of the *RG1* with respect to the observational errors, estimated with Monte Carlo simulations.

The main effects of abundances on the shape of PCMs are clearly summarised in Marino et al. (2019: their figure 27). An enhancement of about 1.2 dex in $[N/Fe]$ explains the vertical extension of SG stars in the region *RG2* on the PCM along the $\Delta col3$ coordinate. A spread of iron affects the position of FG stars along *RG1*.

This simplified scheme, however, does not account for other features of the PCM. The *RG1* is not horizontal but tilted in the PCM, meaning that in principle it must also have a vertical component along $\Delta col3$, the coordinate mainly affected by changes in the N content, the basic feature of the photometric classification of stars into MPs in GCs.

On the other hand, beside a strong component in $\Delta col3$, the *RG2* is showing a noticeable component also along the Δcol . Hence, if the claim by M17 and L22 of a link between the spread in Δcol and iron is sound, there is no reason not to contemplate a metallicity spread also among SG stars.

The comparison shown in Fig. 12 clearly indicates that as the length of the FG sequence in Δcol increases, so does the extension of the *RG2* region populated by SG stars. The corre-

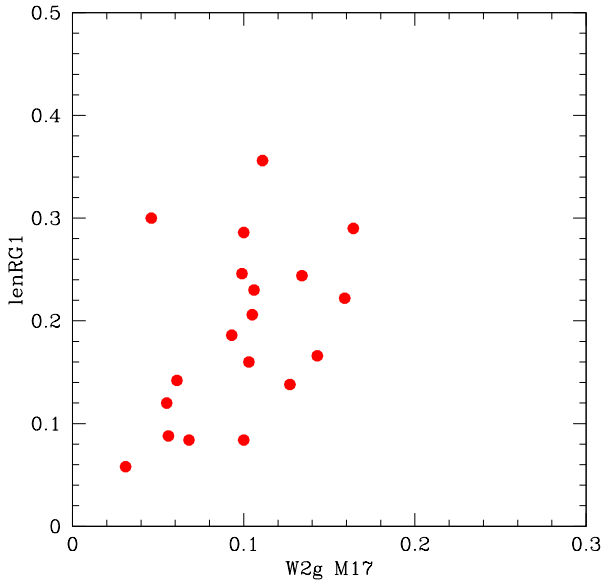


Fig. 14. The extension of the RG1 region as a function of the width of the SG stars (from M17) along the RGB in 20 GCs.

lation has a high statistical significance, hence if the displacement along Δcol has to be associated to a metallicity spread, the logical inference would be to infer a spread in $[Fe/H]$ also in SG stars. From Fig. 12 the comparison between the respective extensions of $RG1$ and $RG2$ is highly significant. The spread of $RG2$ along the Δcol coordinate (supposedly related to the metallicity spread) is not only well comparable to the measured $lenRG1$ values, but in the case of NGC 2808 is clearly much larger than $lenRG1$ itself.

A more thorough comparison can be seen in Fig. 13. In this figure we show the distributions of $RG1$ and $RG2$ in Δcol for the 20 GCs from CB24. In each panel we show the gaussian with σ equal to the rms; the gaussian peaks have been shifted to zero using the mean values, to get an immediate comparison between $RG1$ and $RG2$ distributions (in red and blue, respectively). To complete the comparison, we plot also lines indicating the iqr values for FG and SG stars, using the same colours.

To introduce further complexity, in Fig. 14 the extension of the FG sequence is found to be correlated to the width of the SG stars on the CMD, with high statistical significance (see correlation 7 in Tab. 4). At face value, this means that, were the extension of $RG1$ be really related only to the metallicity spread, the same would be required also to explain the spread of the SG stars on the CMD. Clearly, the scenario depicted by L22 by neglecting the polluted stars in their speculations is too simplistic.

The extensions of the $RG2$ region along the Δcol coordinate in the PCM is correlated to the width $W2g$ of SG stars on the RGB but also to the width $W1g$ of FG stars (left and middle panels in Fig. 15). A statistically significant dependence on the GC metallicity is detected for $iqrSG$ (right panel in Fig. 15).

The extension of $RG2$ in Δcol is plotted as a function of a few other global parameters of GCs in Fig. 16. The correlation with the cluster age is formally not significant ($p=0.055$),

but this result is borderline, since had we used the quantity $rmsSG$, instead, the correlation would have become significant ($p=0.049$), although barely. No clear dependence from the present-day mass of GCs is detected, whereas we found that the extension of $RG2$ seems to depend on the initial mass of GCs (lower left panel in Fig. 16 and correlations 21 and 22 in Table 4). Further studies on the spread in (pseudo-)colours and chemical abundances as their cause are clearly called for also concerning the interpretation of the properties of SG stars.

6. Summary

In the present paper we addressed the issue of the metallicity spreads claimed to be hosted among FG stars in GCs. We investigated the large metallicity spreads in FG GC stars found by L22, surprising in stellar systems formed without an extended star formation. The explanation provided by L22 is based on inhomogeneous mixing during the primary star formation. Afterward, when mixing of polluter matter and pristine gas was used to form the following population of SG, low mass stars, a more thorough homogenisation is predicted to occur, effectively removing any detectable difference in $[Fe/H]$.

We used a large sample of FG stars with spectroscopic abundances and the only available published set of PCMs to match the Δcol position of stars along the $RG1$ sequences. Selecting stars with very similar atmospheric parameters we found no clear correlation between differences in $[Fe/H]$ and displacement in Δcol . Over 30 pairs of stars in 12 GCs, the average shift in Δcol (0.090 mag, $rms=0.114$ mag), which is not statistically significant, is not proportional to the differences in metallicity between the stars in each pair.

For the first time we quantified the real extension of the $RG1$ sequence of FG stars on the PCM. We measured the interquartile range of the extension in Δcol (to alleviate the impact of outliers), the spread in Δcol , $rmsFG$, and the major axis of the ellipse enclosing the FG sequence, $lenRG1$. All these parameters are perfectly consistent with each other. Using these quantitative measurements

1. we did not find any relation between the metallicity spread among FG stars as derived by L22 and the true extension of the region populated by FG stars in the PCM. Globular clusters with very different $RG1$ extensions have identical spreads in $[Fe/H]$ according to L22 (see Fig. 11);
2. the $lenRG1$ values have no significant correspondence also with any estimate of the intrinsic metallicity spread of the GCs as a whole available in the literature. Instead we found that the actual extent of the $RG1$ region in Δcol increases as the average metallicity $[Fe/H]$ of the GCs increases (Fig. 10);
3. the true extension of the $RG1$ sequence, $lenRG1$, is correlated to the width $W1g$ of the FG stars on the RGB in the m_{F814W} versus col plane (Fig. 10), but it is also correlated to the width $W2g$ of the SG stars (Fig. 14). Both these relations have high statistical significance;
4. the $lenRG1$ is very well correlated to the analogous extension in Δcol of the SG sequence. This result should not come unexpected, since the spread of FG stars in col on

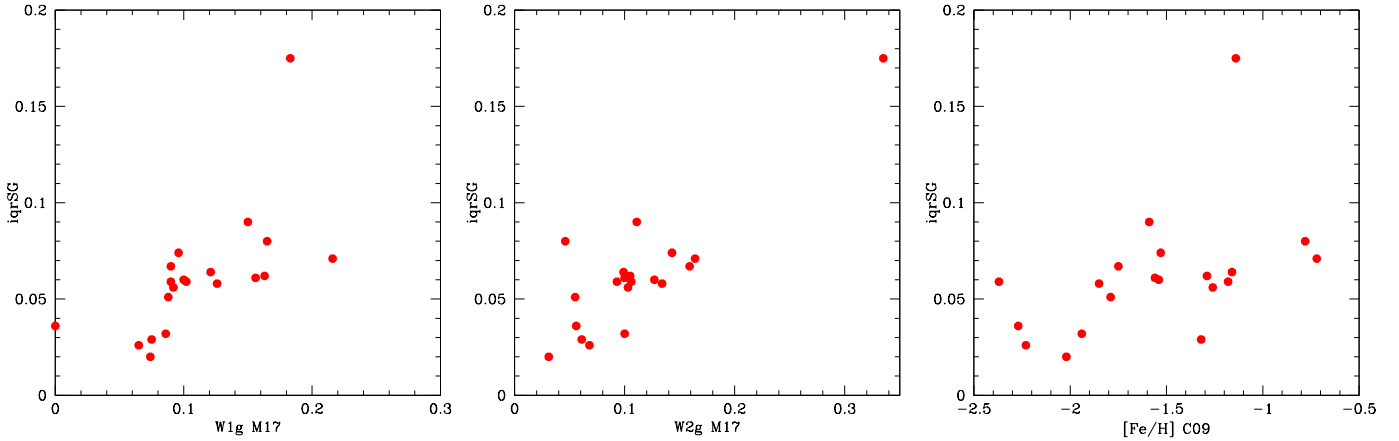


Fig. 15. Extension of the *RG2* region of SG stars as a function of the width of FG stars on the RGB (left panel), the width of SG stars (middle panel), and metallicity [Fe/H] (right panel) in 20 GCs.

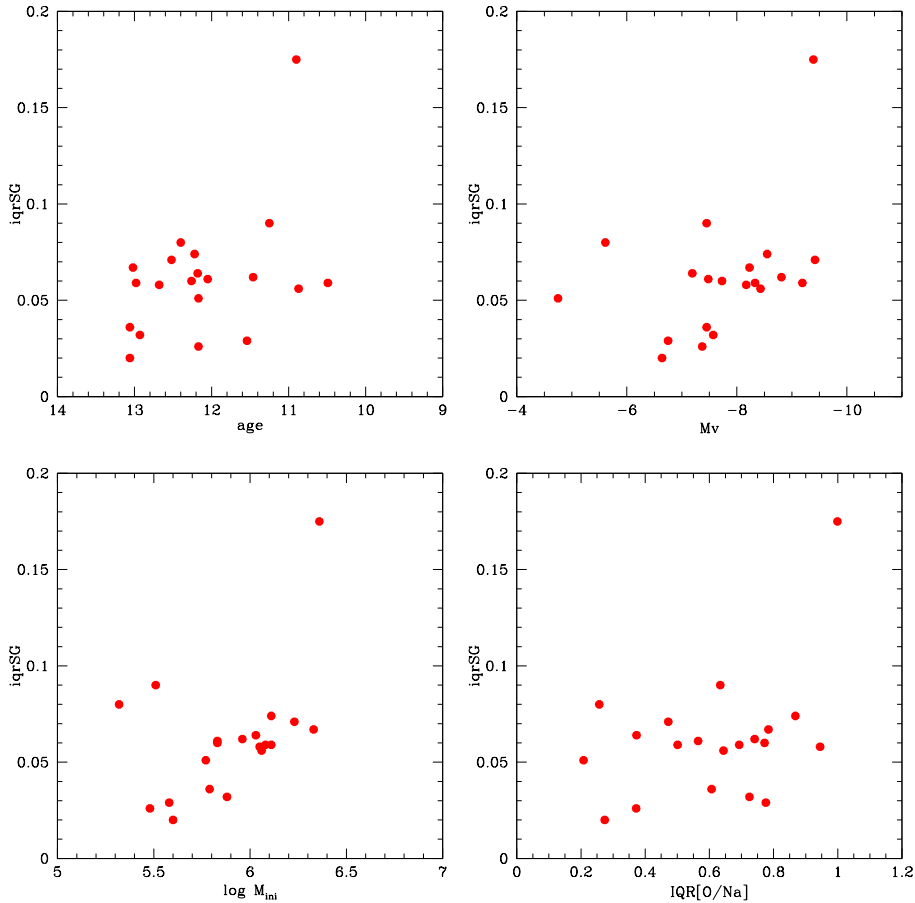


Fig. 16. Extension of the *RG2* region of SG stars in 20 GCs as a function of the GC ages (upper left panel), total absolute magnitude (upper right panel), initial GC mass (lower left panel), and interquartile range of the [O/Na] ratio (lower right panel). References for data sources are listed in Table 4.

the RGB is complementary to the spread of SG stars. The more extended is the location of SG stars, the less is the one of FG stars, and vice versa. When the distance from the fiducial red and blue envelopes of the RGB are used to produce the PCM, the procedure likely provides the statistical significant correlation observed of *lenRG1* to the extent

in Δcol of the *RG2*. This occurrence, neglected by M17, is clearly shown in Fig. 17, where we plotted the correlation of the widths *W1g* and *W2g* from M17. In the figure, GCs analysed in the present paper are depicted as filled symbols, and the correlation is highly significant (correlation 8 in Table 4). However, considering the whole sample of 56

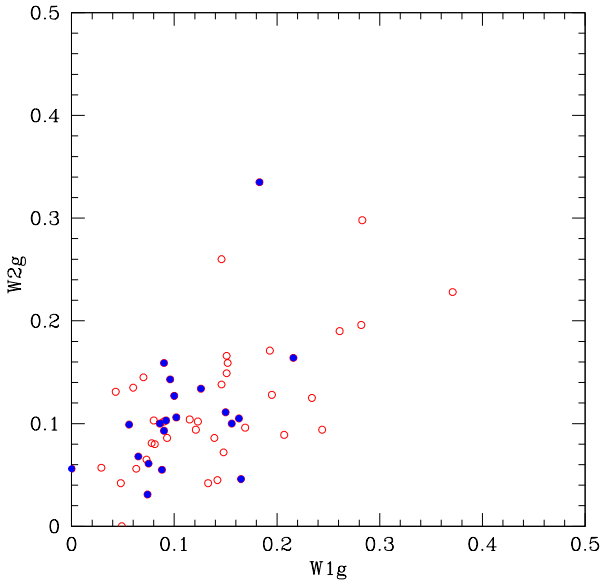


Fig. 17. Correlation of the width $W1g$ of FG stars in col and the width $W2g$ of SG stars for the 56 GCs in M17. The GCs in the subsample by CB24 utilised in the present paper are plotted as filled blue symbols.

GCs tabulated in M17, the correlation of $W1g$ with $W2g$ is even more significant (Pearson's correlation coefficient $r=0.652$, $p < 1.0 \times 10^{-6}$), a fact not mentioned either in M17 or in L22;

5. the extension in Δcol of the $RG2$ presents significant relations with the cluster average metallicity $[Fe/H]$ and the total GC mass, either the present-day mass or the initial mass before any dynamical evolution onset. The correlation between the extension of $RG2$ and the GC age is more uncertain, being barely statistically significant.

The implications of our findings challenge the scenario depicted by L22 and M17. If the extension of $RG1$ has to be related to a metallicity spread, then the same must be true also for SG stars. We should observe a metallicity spread in any population of GC stars, occurrence which is neither mentioned by L22, M17 nor observed in most GCs. Vice versa, the tight correlation between the spread in Δcol in $RG1$ and $RG2$ implies that if no metallicity spread is present among SG stars, then it hardly should be existing among FG stars. The good agreement between spreads in Δcol in $RG1$ and $RG2$, highlighted for the first time thanks to quantitative measurements of their extension in the PCMs, indicates that no significant difference is present concerning the homogeneity of the intracluster medium from which the primary star formation formed the FG stars and the following phase of formation of SG stars, invalidating the scenario proposed by L22.

Finally, since the extension of $RG1$ and $RG2$ increases as the width of FG and SG stars increases on the RGB, this probably means that $W1g$ and $W2g$ are reasonable estimates. It is likely the conversion of these width into spread of $[Fe/H]$ to be the problem.

Acknowledgements. We thank the referee for careful and useful comments and suggestions. This research has made use of the VizieR catalogue access tool, CDS, Strasbourg, France (DOI: 10.26093/cds/vizieer). The original description of the VizieR service was published in 2000, A&AS 143, 23. Use of the NASA's Astrophysical Data System, and TOPCAT (Taylor 2005) are also acknowledged.

References

- Bailin, J. 2019, ApJS, 245, 5
 Bailin, J., von Klar, R. 2022, ApJ, 925, 36
 Bastian, N., Lardo, C. 2018, ARA&A, 56, 83
 Battaglia, G., Tolstoy, E., Helmi, A. et al. 2006, A&A, 459, 423
 Baumgardt, H., Hilker, M., Sollima, A., Bellini, A. 2019, MNRAS, 482, 5138
 Bekki, K., Freeman, K.C. 2003, MNRAS, 346, L11
 Boberg, O.M., Friel, E.D., Vesperini, E. 2016, ApJ, 824, 5
 Bragaglia, A., Carretta, E., D'Orazi, V. et al. 2017, A&A, 607, A44
 Calamida, A., Bono, G., Stetson, P.B. et al. 2007, ApJ, 670, 400
 Carretta, E. 2015, ApJ, 810, 148
 Carretta, E., Bragaglia, A. 2024, A&A, 690, A158
 Carretta, E., Gratton, R.G., Clementini, G., Fusi Pecci, F. 2000, ApJ, 533, 215
 Carretta, E., Bragaglia, A., Gratton R.G., et al. 2006, A&A, 450, 523
 Carretta, E., Bragaglia, A., Gratton, R.G., D'Orazi, V., Lucatello, S. 2009a, A&A, 508, 695
 Carretta, E., Bragaglia, A., Gratton, R.G. et al. 2009b, A&A, 505, 117
 Carretta, E., Bragaglia, A., Gratton, R.G., Lucatello, S. 2009c, A&A, 505, 139
 Carretta, E., Bragaglia, A., Gratton, R.G. et al. 2010, ApJ, 714, L7
 Carretta, E., Bragaglia, A., Gratton, R.G., D'Orazi, V., Lucatello, S. 2011a, A&A, 535, 121
 Carretta, E., Lucatello, S., Gratton, R.G., Bragaglia, A., D'Orazi, V. 2011b, A&A, 533, 69
 Carretta, E., Bragaglia, A., Gratton, R.G. et al. 2014, A&A, 564, A60
 Carretta, E., Bragaglia, A., Gratton, R.G. et al. 2015, A&A, 578, A116
 Cohen, J.G., Melendez, J. 2005, AJ, 129, 303
 Dopita, M.A., Smith, G.H. 1986, ApJ, 304, 283
 Dotter, A., Chaboyer, B., Jevremovic, D. et al. 2007, AJ, 134, 376
 Fanelli, C., Origlia, L., Rich, R.M. et al. 2024, A&A, 690, A139
 Gaia Collaboration, Brown, A. G. A., Vallenari, A., et al. 2018a, A&A, 616, A1.
 Gaia Collaboration, Helmi, A., van Leeuwen, F., et al. 2018b, A&A, 616, A12.
 Gaia Collaboration, Vallenari, A., Brown, A.G.A., et al. 2023, A&A, 674, A1.
 Gratton, R.G., Bonifacio, P., Bragaglia, A., et al. 2001, A&A, 369, 87
 Gratton, R.G., Sneden, C., Carretta, E. 2004, ARA&A, 42, 385
 Gratton, R.G., Carretta, E., Bragaglia, A. 2012, A&ARv, 20, 50
 Gratton, R.G., Bragaglia, A., Carretta, E., D'Orazi, V., Lucatello, S., Sollima, A. 2019, A&ARv, 27, 8
 Harris, W.E. 2010, ArXiv, 1012.3224
 Johnson, C.I., Rich, M.R., Pilachowski, C.A. et al. 2015, AJ, 150, 63
 Johnson, C.I., Calamida, A., Kader, J.A. et al. 2023, AJ, 163, 3
 Kirby, E.N., Guhathakurta, P., Simon, J.D. et al. 2010, ApJS, 191 352
 Kirby, E.N., Lanfranchi, G.A., Simon, J.D., Cohen, J.G., Guhathakurta, P. 2011, ApJ, 727, 78
 Kruijssen, J.M.D., Pfeffer, J.L., Reina-Campos, M., Crain, R.A., Bastian, N. 2019, MNRAS, 486, 3180
 Langer, G.E., Hoffman, R., Sneden, C. 1993, PASP, 105, 301
 Lardo, C., Bellazzini, M., Pancino, E. et al. 2011, A&A, 525, A114
 Lardo, C., Salaris, M., Cassisi, et al. 2023, A&A, 669, A19

- Lee, J.-W., Lee, J., Kang, Y.-W. et al. 2009, *ApJ*, 695, L78
- Legnardi, M.V., Milone, A.P., Armillotta, L. et al. 2022, *MNRAS*, 513, 735
- Legnardi, M.V., Milone, A.P., Cordini, G. et al. 2024, *A&A*, 687, A160
- Leitinger, E., Baumgardt, H., Cabrera-Ziri, I., Hilker, M., Pancino, E. 2023, *MNRAS*, 520, 1456
- Marino, A.F., Villanova, S., Piotto, G. et al. 2008, *A&A*, 490, 625
- Marino, A.F., Milone, A.P., Sills, A. et al. 2019, *ApJ*, 887, 91
- Milone, A.P., Piotto, G., Renzini, A. et al. 2017, *MNRAS*, 464, 3636
- Nardiello, D., Libralato, M., Piotto, G. et al. 2018, *MNRAS*, 481, 3382
- Salaris, M., Cassisi, S., Weis, A. 2002, *PASP*, 114, 375
- Sbordone, L., Salaris, M., Weiss, A., Cassisi, S. 2011, *A&A*, 534, A9
- Siegel, M.H., Dotter, A., Majewski, S.R. et al. 2007, *ApJ*, 667, L57
- Snedden, C., Kraft, R.P., Guhathakurta, P., Peterson, R.C., Fulbright, J.P. 2004, *AJ*, 127, 2162
- Stetson, P.B., Pancino, E., Zocchi, A., Sanna, N., Monelli, M. 2019, *MNRAS*, 485, 3042
- Taylor, M.B. 2005, *Astronomical Data Analysis Software and Systems XIV*, 347, 29
- VandenBerg, D.A., Brogaard, K., Leaman, R., Casagrande, L. 2013, *ApJ*, 775, 134
- Willman, B., Strader, J. 2012, *AJ*, 144, 76

Appendix A: Selected samples of FG and SG stars in the program GCs

We present here the selection of FG and SG stars (i.e., the populations of the *RG1* and *RG2* regions, respectively) for the 20 GCs discussed in the present paper. We used the PCMs derived by CB24 and isolated *RG1* and *RG2* stars manually, using TOPCAT; the result of the selection is shown in the following figures (from Fig. A.1 to Fig. A.5), where FG stars are coloured in red and SG stars are coloured in blue, respectively. Stars falling far from the main distributions in the CMDs, and consequently in the PCMs, were ignored; they are always a minority and are indicated in grey in the plots. In each plot we also show the ellipse enclosing the *RG1* (in black) with the major axis measuring the actual extension of *RG1* drawn in green. Information on the extension of the *RG1* and its inclination is given in Table 4 in the main text.

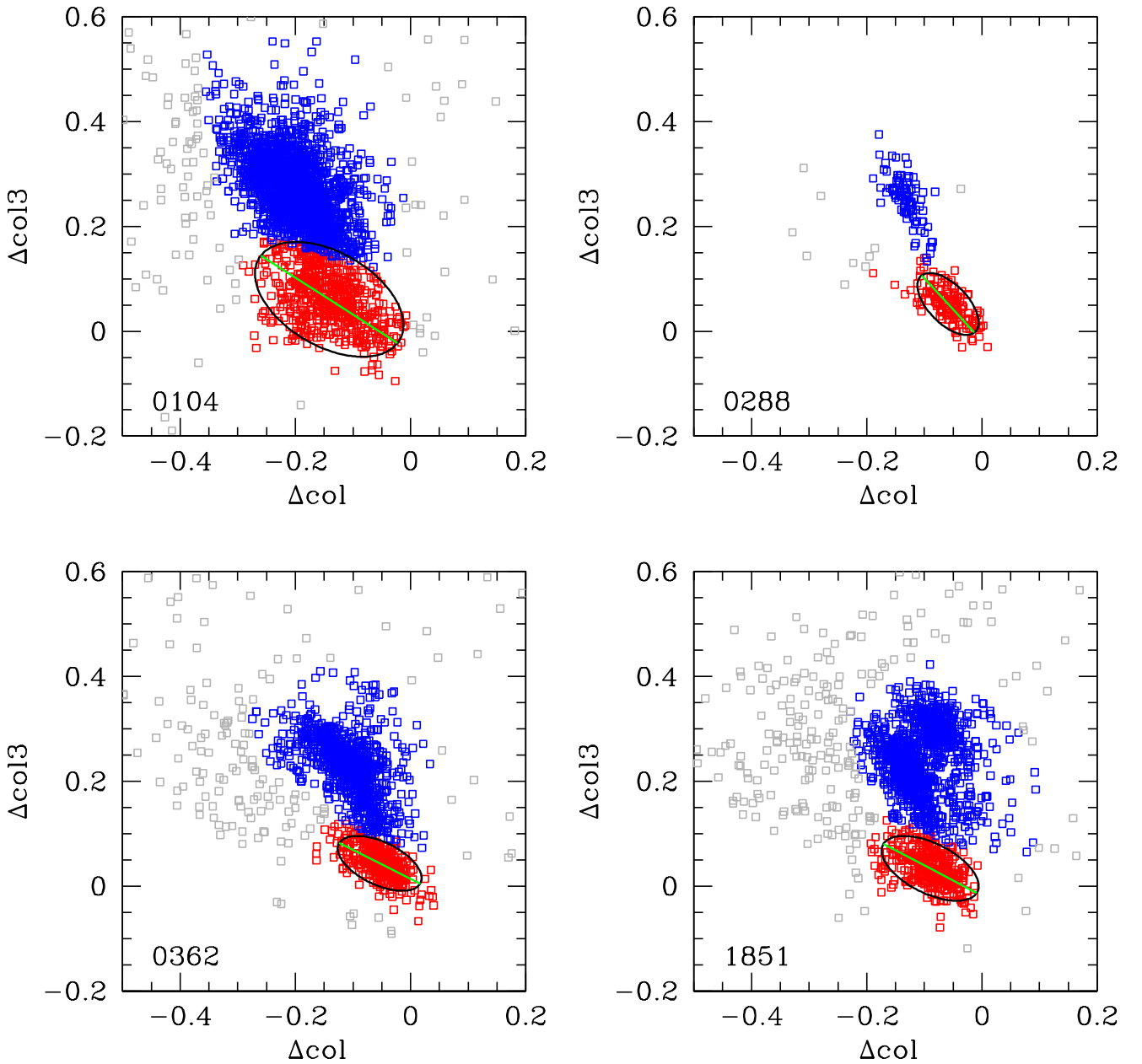


Fig. A.1. Separation of FG and SG stars (in red and blue, respectively) in the PCMs of the four clusters NGC 0104, NGC 0288, NGC 0362, and NGC 1851. The ellipses indicate the *RG1* region.

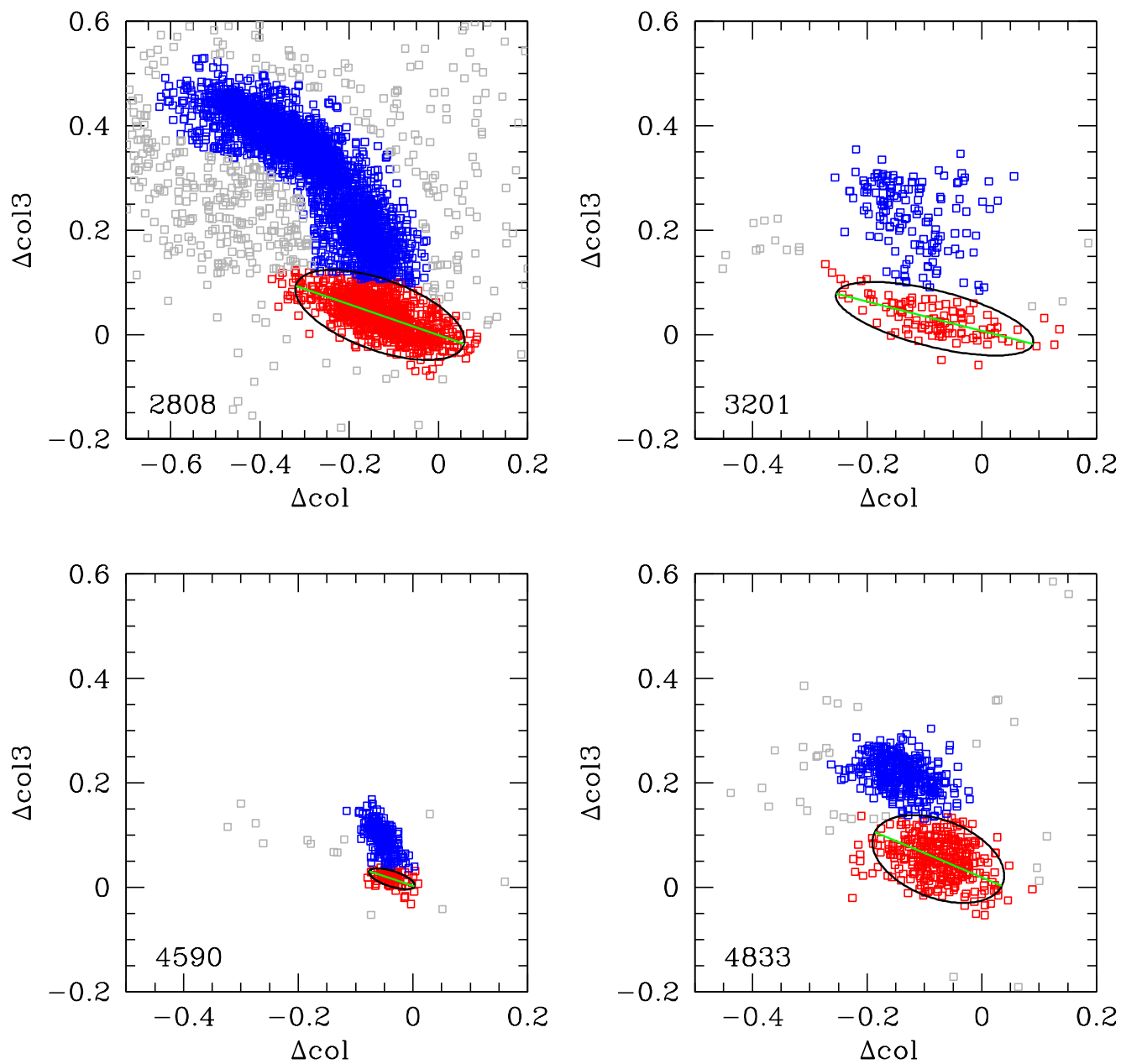


Fig. A.2. The same, for NGC 2808 (notice the slightly different x-axis scale), NGC 3201, NGC 4590, and NGC 4833.

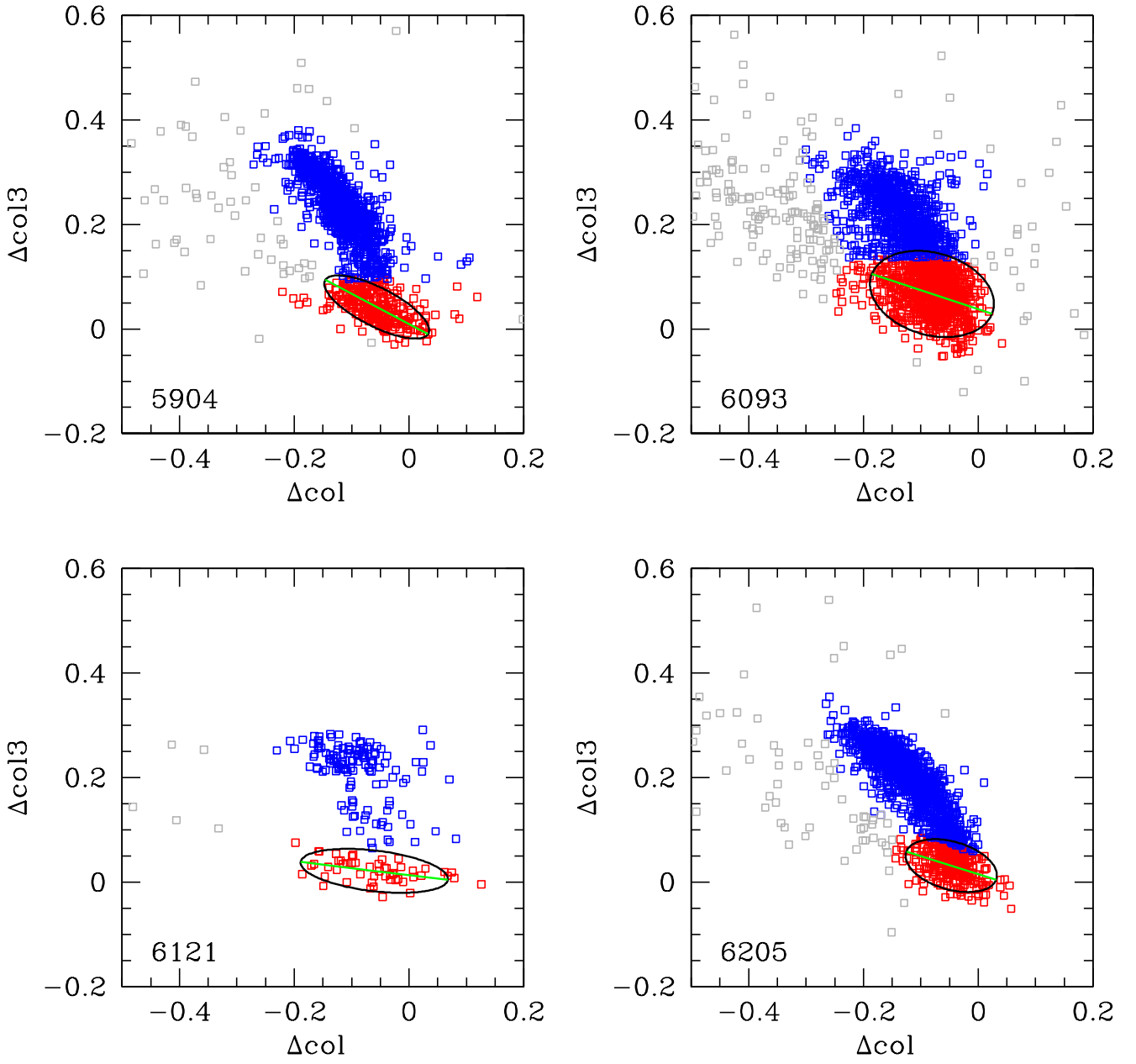


Fig. A.3. The same, for NGC 5904, NCGC 6093, NGC 6121, and NGC 6205.

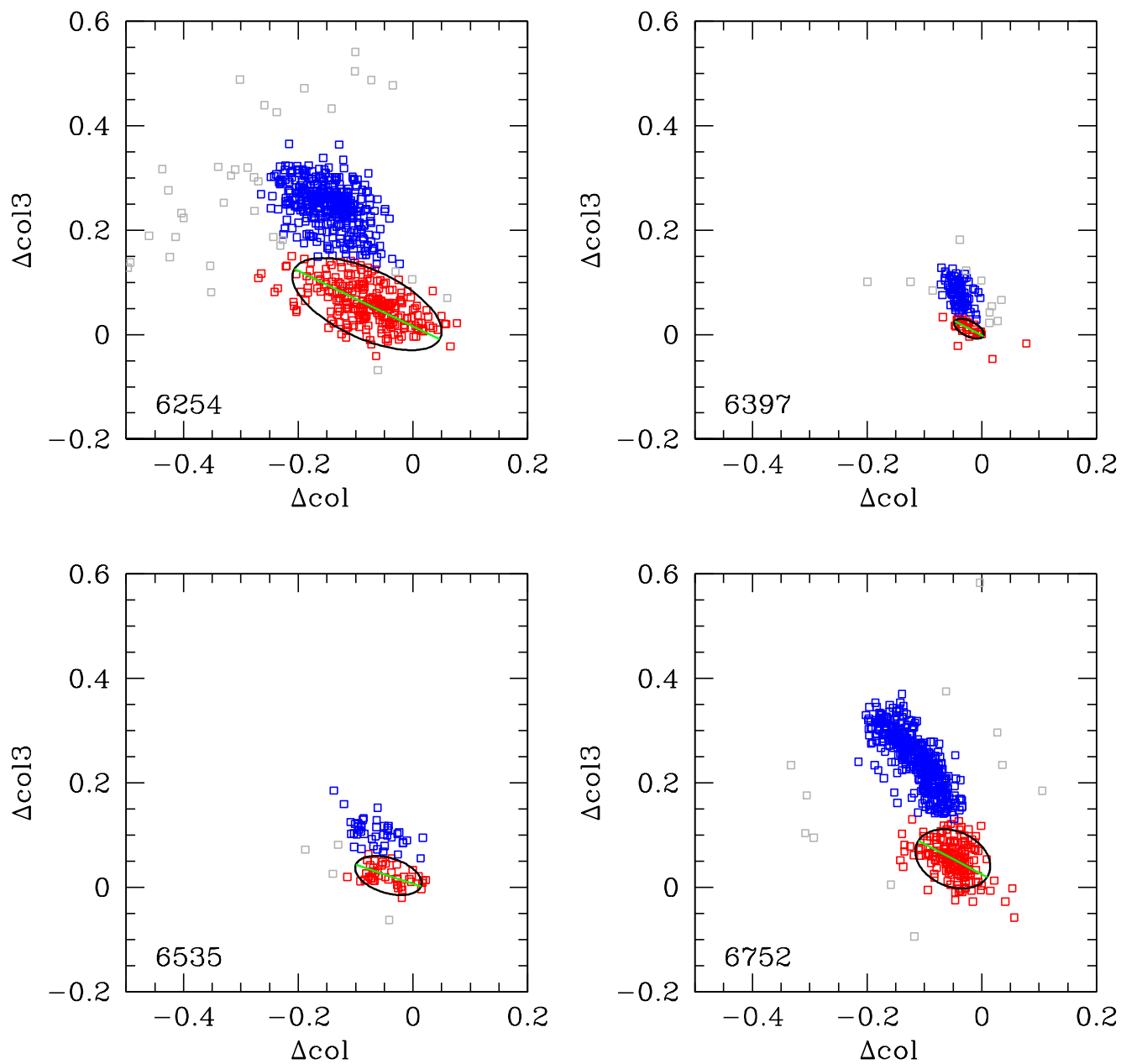


Fig. A.4. The same, for NGC 6254, NCGC 6397, NGC 6535, and NGC 6752.

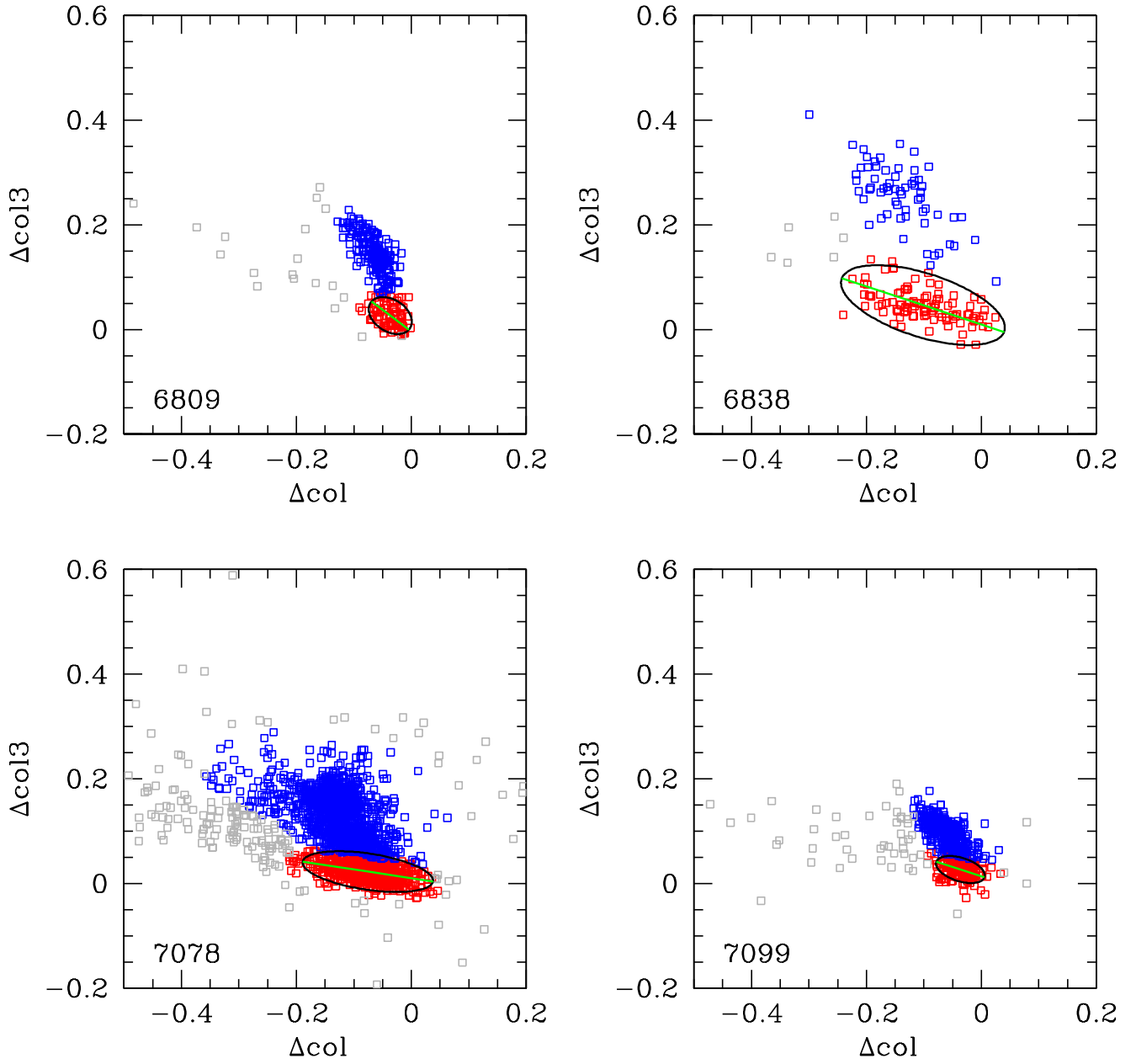


Fig. A.5. The same, for NGC 6809, NCGC 6838, NGC 7078, and NGC 7099.